Trapping AsPh3 via reaction with NiS/γ-Al2O3 in the presence of H2: Reaction mechanism and kinetics

Angelique Jallais, Michel Thomas, Antoine Hugon, Igor Bezverkhyy

Trapping $AsPh_3$ via reaction with $NiS/\gamma\text{-}Al_2O_3$ in the presence of H_2: reaction mechanism and kinetics

Angélique Jallais,[a] Michel Thomas,[a] Antoine Hugon,[a] Igor Bezverkhyy[b*]

[a] IFP Energies nouvelles, Rond-point de l'échangeur de Solaize, BP 3, 69360, Solaize, France

[b] Laboratoire Interdisciplinaire Carnot de Bourgogne, UMR 6303 CNRS-Université de Bourgogne Franche-Comté, BP 47870, 21078 Dijon Cedex, France

*Corresponding author

Abstract

Removal of As from petroleum feedstocks is an important process which can be realized using As trapping mass containing supported nickel sulfide. In order to understand the mechanism of the trapping we studied the reaction of $AsPh_3$ with $NiS/\gamma\text{-}Al_2O_3$ in the presence of H_2 in a batch reactor in toluene solution at 230°C. This reaction results in formation of NiAs, benzene and H2S. Also, the intermediate species, thiophenol and diphenylsulfide, were observed. Despite formation of NiAs layer in the course of reaction, the rate of $AsPh_3$ decomposition is not affected by the solid state diffusion up to ~ 50% of nickel conversion. The rate determining step in these conditions appears to be the hydrogenolysis of As-C bonds. It was found that the reaction order changes in the course of reaction from zero to one. This trend is described by a kinetic model assuming adsorption of $AsPh_3$ molecules followed by decomposition.

Keywords: As trapping mass, protection of hydrotreatment catalysts, dearsenification

1. Introduction

Arsenic can be naturally found in crude oils at very low concentrations, often comprised between 10 and 200 $\mu g.kg^{-1}$ (10-200 ppb) [1,2] as determined by graphite furnace atomic absorption spectrometry (GF-AAS). It can also be found in distillation cuts, gas condensates [3] or feed streams treated in catalytic processes, mainly as organic arsenic compounds AsR_3.

It is known that organic arsenic can be a severe poison for different types of catalysts [4]. It has been shown that arsenic can poison nickel steam reforming catalysts forming NiAs or Ni_5As_2 as a final phase [5]. It has also been proved that As is a strong poison of hydrotreating catalyst such as sulfided $CoMo/Al_2O_3$ [6] which is used to decrease the S content below 10 ppm of FCC gasoline in order to meet commercial specifications.

Two studies have been realized to understand the mechanism of As poisoning in hydrotreating catalysts [7-8]. A deactivated $NiMoP/Al_2O_3$ hydrotreating catalyst was characterized by EXAFS in the work of Puig-Molina et al. [7]. The studied material was exposed to few ppb levels of As for several years in an industrial reactor and was resulfided before the EXAFS measurements. It was concluded about the possible formation of As_2S_3 but the formation of As-Ni bonds was not observed. Also, the authors suggest that the deactivation of the catalyst by As could be explained by the formation of Ni-S-As bounds leading to the blockage of Ni sites.

Nelson et al. [8] studied the arsenic poisining of NiMoS catalyst by DFT. It has been shown that As-containing molecules (AsH_3, trimethylarsine (TMA), triethylarsine (TEA), triphenylarsine (TPA)) can be adsorbed through the As atom onto the catalyst Ni atoms. The dissociation of arsenic compounds on NiMoS surface was studied and it was shown that the dissociation energy increases in the order AsH_3 < TPA < TEA < TMA, indicating a strong influence of the ligand nature on the reactivity of arsenic species. This study also showed that As atoms can be incorporated into the NiMoS catalyst through substitution of Ni or S atoms.

In order to protect HDS catalysts from poisoning by As, arsenic trapping masses have been developed which are based on nickel deposited on alumina [9]. They may be placed either in a separate guard bed upstream the HDT unit or in the same bed as the catalyst close to the entry of the feed. In this case, the operating conditions (temperature, hydrogen pressure, residence time) are fixed by the catalytic section. The trapping mass can be sulfided either prior to use or in situ by traces of H_2S or sulfur-containing molecules present in the feed.

The information about the mechanism of As trapping by these masses is very scarce. Only the reaction between Ni^0 and TPA in H_2 atmosphere has been studied by Ryndin et al. in a series of works [10-14]. It has been found that after a sufficient time of contact the metallic nickel was completely transformed into a single phase of NiAs (nickeline) and the mechanism for this reaction has been proposed. It proceeds through TPA adsorption on the surface sites followed by the hydrogenolysis of the As-C bounds with the formation of benzene and cyclohexane. Finally, migration of the As atom into the bulk of Ni^0 particles produces NiAs. Despite the importance of these results, they are not relevant to industrially used As trapping masses, since these materials contain Ni in sulfided and not in metallic form. In order to get a better understanding of the mechanism of As trapping by nickel sulfide, we studied in the present work the reactivity of NiS supported on alumina towards As-containing species.

Given a variety of As species present in different petroleum cuts, the choice of the representative species is not straightforward. We decided to study the reactivity of triphenylarsine (TPA or $AsPh_3$) as in the previous works [10-14]. Although the boiling temperature of this compound (360 °C) exceeds that of FCC gasoline (50-220°C), we chose TPA for two reasons. First, it is commercially available in a highly pure form and due to its low volatility it can be easily handled. Second, its use permits direct comparison of our results with those obtained for metallic nickel. To evaluate the effect of ligands on the reactivity we performed some additional experiments using triethylarsine ($AsEt_3$, TEA, T_{nbp} = 140 °C) under similar reaction conditions.

2. Experimental

2.1. Synthesis of NiS/γ-Al_2O_3 trapping mass

A mesoporous γ-Al_2O_3 in the form of extrudates with a surface area of 270 m^2/g was used as the support for the synthesis (the material was kindly provided by Axens, France). The NiO/Al_2O_3 precursor was prepared by the incipient wetness impregnation method using $Ni(NO_3)_2.6H_2O$ as nickel source (Alfa Aesar, 99.9985%). An amount of 20.81 g of nickel nitrate was dissolved in 15 mL of water then slowly dropped onto 25.80 g of dried alumina in a rotating beaker in order to soak the entire solid. It was then stored 24 hours under wet atmosphere to allow the diffusion of the nickel species into the alumina porosity and dried overnight in an oven at 100 °C. The calcination step was then performed at 450 °C for 2 hours under air.

A sample of NiO/Al_2O_3 was kept at this point and another was reduced under H_2 in order to obtain Ni^0/Al_2O_3. The rest of the NiO/Al_2O_3 was then sulfided under a flowing mixture of H_2S/H_2 (15 % v/v, Air Products) at 200 °C for 2 hours, at 350 °C for 1 hour and at 200 °C for 2 hours under H_2 only in order to remove the excess of sulfur. The sulfided solids were kept under argon.

2.2 Test of $AsPh_3$ trapping

The chemicals used in the study were obtained from the following providers: triphenylarsine (Sigma Aldrich, 97 %), triethylarsine (Strem chemicals, 98%), toluene (VWR chemicals, 99.8 %).

The reaction of triphenylarsine (TPA) with the synthesized trapping masses was carried out in a batch reactor, stirred by a mechanical agitator, in 250 mL of toluene, at 230 °C and under hydrogen pressure of 23 bar. Prior to the test, the desired amount of trapping mass was placed into the reactor under argon atmosphere, covered with toluene, and then the reactor was purged and pressurized with H_2. The temperature and the pressure of the reactor were established at the desired values and a known amount of TPA in toluene was introduced into the reactor using a connected charge vessel, pressurized with H_2 as well. A scheme of the unit can be seen in Fig.1.

In order to find conditions free of kinetic limitations due to internal and external mass transfer, the

experiments have been realized with different particle size in the range 0.4 – 3 mm. We have found that no limitations exist for particles smaller than 800 μm, therefore the particle fraction between 600 and 800 μm was used in the present study. Also, it was verified that the rate of reaction did not depend on the stirring rate, fixed at 1000 rpm. In addition to these experiments, the blank measurements were performed which showed that pure γ-Al_2O_3 is not active in $AsPh_3$ transformation in the used operation conditions (Fig.S1).

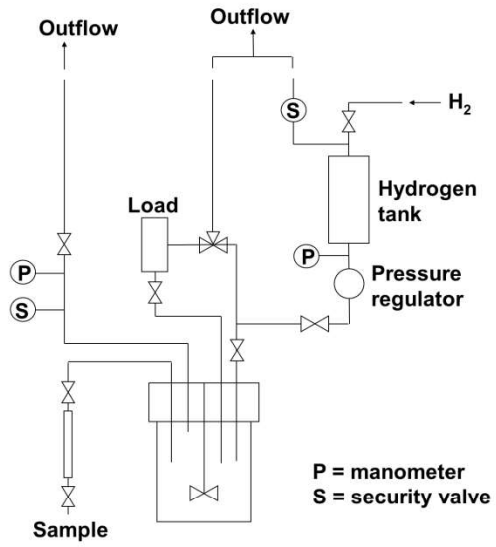

Figure 1 Scheme of the experimental setup used for the tests of $AsPh_3$ trapping in a batch reactor in H_2 atmosphere (see text for details).

The concentrations of TPA and of the reaction products in the solution were analyzed at regular intervals of time by gas-phase chromatographic analysis using an apparatus from Agilent. Injection was performed at 150°C with an injection volume of 0.2 μL. The column used for the separation was an Agilent DB-5 (30m x 0.32mm x 0.25μm) and detection was performed with a flame ionization detector (FID). Additional experiments were performed under different conditions in order to determine the relative standard errors of the concentration measurements. The following values were obtained: 6 % for triphenylarsine, 15 % for thiophenol (PhSH), 12 % for diphenylsilfide (Ph_2S) and 6 % for thriethylarsine ($AsEt_3$).

2.3 Characterization techniques

The XRD measurements were performed using a Panalytical X'Pert Pro diffractometer with a

Bragg-Brentano geometry using nickel-filtered Cu-Kα radiation (λ = 0.15406). In order to avoid any oxidation of the solids after the test, the samples were prepared in a glovebox under argon and the XRD cells were sealed with Kapton tape. For *in situ* XRD measurements during the sulfidation step the XRK 900 chamber from Anton Paar has been used. The protocol included a first step under a flowing mixture of H_2S/H_2 (15 % v/v) at 200 °C for 2 hours, then at 350 °C for 1 hour and finally at 200 °C for 2 hours under H_2 flow. Two measurements were done at each step of the sulfidation. The XRF measurements of the liquids and solids were performed using two wavelength dispersive X-ray fluorescence spectrometers, from Panalytical and Thermo Fisher Scientific. X-ray Photoelectron spectroscopy (XPS) was applied in order to determine surface composition of samples using the apparatus PHI 5000 Versaprobe with monochromatic Al Kα1 radiation. The samples were transferred to the XPS chamber under inert atmosphere. Transmission electron microscope images were recorded on a transmission electron microscope JEOL JEM-2100 under an accelerating voltage of 200 kV.

3. Results and discussion

3.1 Properties of the trapping mass

Considering the air sensitivity of the solids, determination of the nickel loading was performed before the sulfidation step using X-ray fluorescence. An average value of 13.8 Ni % (w/w) was determined for the different batches of the prepared trapping mass. The dispersion of Ni^0 (surface nickel atoms per total nickel atoms) was also measured using hydrogen chemisorption after reduction (410 °C for 16 hours then under vacuum at 350 °C for 3 hours). Assuming the stoichiometry of one chemisorbed hydrogen atom per surface nickel atom, a dispersion of 13 % was obtained.

To determine the crystalline phases formed during the synthesis the solids were analyzed by *in situ* XRD during the sulfidation step. As shown in Fig.2, after 2 hours at 350 °C under a flowing mixture of H_2S/H_2 (15% v/v), the observed phases are NiS (NiAs type) and γ-Al_2O_3. Applying the Debye-Scherrer equation to (2-10) diffraction peak of NiS (2θ = 53°) we found that the size of NiS

crystallites is 9 ± 0.9 nm. TEM was also applied to characterize the microstructure of the sample (Fig.S2). NiS particles can be distinguished on the images as darker regions, but unfortunately due to a poor contrast between NiS and γ-Al_2O_3 a detailed analysis of particle shape and size distribution was not possible.

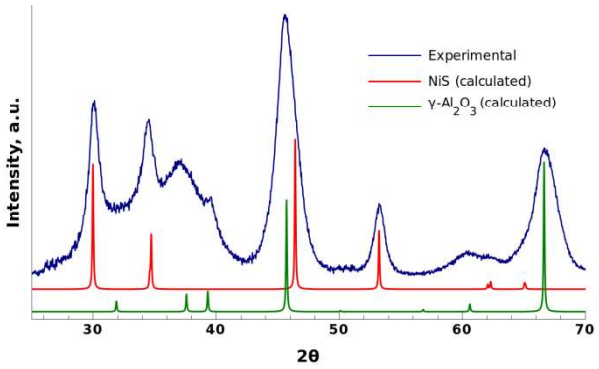

Figure 2 *In situ* XRD pattern of NiS/γ-Al_2O_3 sample used in the work.

The solids were analyzed by XRF in order to determine the mass percentage of nickel and sulfur. The results were 13.3 % for nickel and 5.7 % for sulfur which gives a S/Ni molar ratio of 0.8. Since the only observed Ni-S phase is NiS (NiAs type), this result suggests that part of the nickel oxide is not transformed during the sulfo-reduction step and that the NiS phase coexists with the remaining nickel oxide.

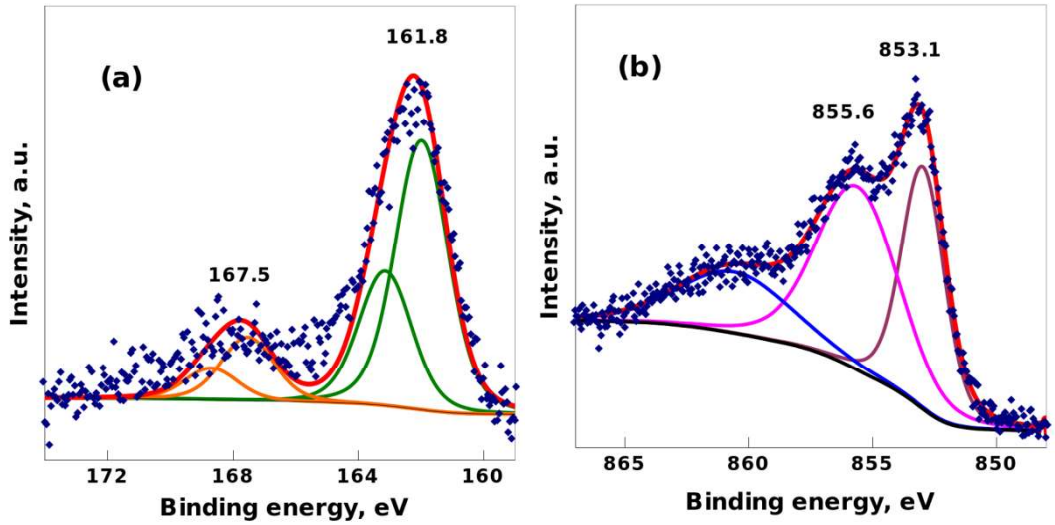

Figure 3 S 2p (a) and Ni $2p_{3/2}$ (b) narrow scan XPS spectra of NiS/γ-Al_2O_3 sample used in the work.

XPS results are in line with the XRD pattern and elemental analysis (Fig.3). S2p spectrum can be described by a sum of two unresolved doublets consisting of $S2p_{1/2}$ and $S2p_{3/2}$ peaks. The position of the main $S2p_{3/2}$ peak (161.8 eV) corresponds to S^{2-} in NiS [15]. A low intensity peak at 167.5 eV can be attributed to sulphate species formed after contact with trace amount of oxygen. Ni $2p_{3/2}$ spectrum can be described by a sum of two peaks with binding energies of 853.1 eV and 855.6 eV (a low intensity peak at ~ 861 eV corresponds to a satellite). The low energy component corresponds to Ni atoms in sulfur environment and the high energy one is characteristic of Ni^{2+} oxo or hydroxo species [15,16]. The presence of Ni-O species in XPS spectra and the value of the obtained atomic S/Ni ratio (0.75) confirm the presence of NiO in our sulfide sample.

3.2. Characterization of the products obtained after $AsPh_3$ trapping

The main reaction product in the liquid phase is benzene which represents more than 95 % of the species produced in the liquid phase after a complete decomposition of $AsPh_3$. Two intermediate species were also detected in the course of reaction: thiophenol (PhSH) and diphenylsulfide (Ph_2S) (Fig.4). Using these products yields the carbon balance close to 100 % suggesting that no other organic species were formed in significant concentration.

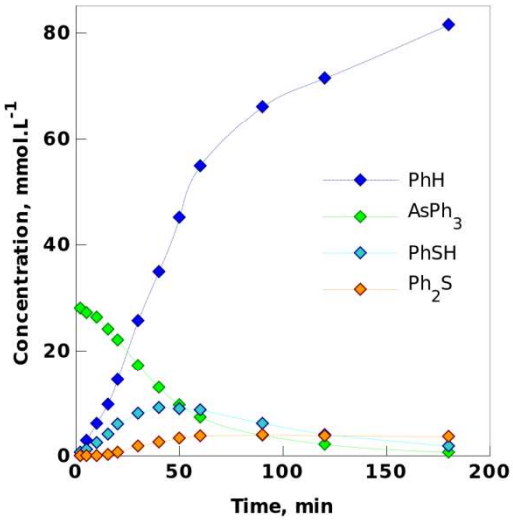

Figure 4 Concentration of the reaction products in the liquid phase as a function of time during reaction of $AsPh_3$ with NiS/γ-Al_2O_3 (As/Ni initial ratio – 1, 230°C, 23 bar H_2). The lines are guides for the eyes.

In contrast to solid products, the composition of the liquid phase could be measured as a function of time revealing different trends for the detected species. While the amount of benzene increases with time, the trends for the other products are more complex (Fig.4). The concentration of thiophenol passes through the maximum and that of diphenylsulfide achieves a plateau after certain time. For the experiment with As/Ni = 1 the time course of all products changes after ~ 50 min of reaction corresponding to decomposition of ~ 50% of the initial amount of $AsPh_3$. The origin of this change will be discussed in detail in section 3.5.

The sulfur content of the spent sorbent decreases when As/Ni ratio rises due to substitution of sulfur in NiS by arsenic during reaction (Table 1). However, the sulfur content of the liquid and solid phases does not correspond to the initial sulfur amount in the sorbent (Table 1). This effect can be due to formation of gaseous sulfur-containing species. Unfortunately the configuration of our test setup does not allow a quantitative analysis of the gas phase. Nevertheless, a gas sample was collected and analyzed using the gas chromatograph equipped with a sulfur specific FPD detector and the presence of H_2S was qualitatively confirmed.

Table 1 As and S concentrations in liquid and solid phases after the end of the test for different initial concentrations of $AsPh_3$

Concentration of $AsPh_3$		As/Ni initial molar ratio	Initial As amount, mmol	As, mmol		As balance	Initial S amount mmol (in NiS/Al_2O_3)			S balance
mmol/L	ppmw(As)			solid	liquid			solid	liquid	
28.6	2500	1	7.2	6.1	0.8	0.96	5.5	1.1	1.94	0.55
11.4	1000	0.4	2.9	2.7	nd	0.93	5.5	2.8	0.22	0.54
5.7	500	0.2	1.4	1.4	nd	1.0	5.5	3.6	nd	0.66
2.9	250	0.1	0.7	0.7	nd	1.0	5.5	4.6	nd	0.84
1.1	100	0.04	0.3	0.3	nd	1.0	5.5	5.1	nd	0.93

nd – not detected

In contrast to sulfur, the arsenic balance is close to unity (Table 1) evidencing that the reaction does

not produce any gaseous As species. Moreover, except at the highest used concentration, no As-containing species were found in the liquid phase. This finding shows that for the concentrations below 1000 ppm all the arsenic initially present in the solution is trapped on the sorbent. This observation is important from the application point of view. It means that in the industrially relevant concentration range (< 1 ppm) the use of NiS/Al_2O_3 could allow to trap all present arsenic on the solid sorbent without producing any gaseous or liquid phase As species.

To determine the nature of As-containing phase, we characterized by XRD the spent sorbent after reaction at the highest $AsPh_3$ concentration (Fig.5). The only arsenide phase detected in the pattern is NiAs (nickeline) whose crystallite size (9±1 nm) is very close to that of the initial NiS. For the trapping masses used in the tests with lower $AsPh_3$ concentrations the peaks of NiAs were not detected in the XRD patterns. This observation can be explained by the low amount of NiAs in these cases and/or by the small size of the crystallites in the partially converted samples.

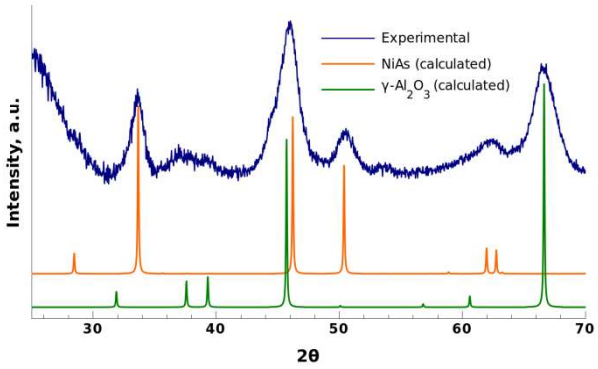

Figure 5 XRD pattern of $NiS/\gamma\text{-}Al_2O_3$ sample after a complete reaction with $AsPh_3$ ($AsPh_3$ initial concentration – 28.6 $mmol.L^{-1}$, As/Ni = 1, 230°C, 23 bar H_2).

In order to better describe the microstructure of the formed NiAs phase, the sample obtained after reaction was characterized by TEM (Fig.6, left panel). The typical low resolution image shows that the size of the formed NiAs particles varies in a wide range, from ~ 2 nm to more than 20 nm. The high resolution image of a large particle pointed by an arrow (Fig.6, right panel) shows the origin of this variability. The larger particles are polycrystalline consisting of smaller crystallites whose size is closer to that determined by XRD. The Fourier transform of the high resolution image shows the

presence of the lattice planes families with the distances characteristic of NiAs: 2.66 Å (101), 1.81 Å (2-10), 1.33 Å (202) and 1.14 Å (203). This fact confirms unambiguously our conclusion about formation of NiAs based on XRD.

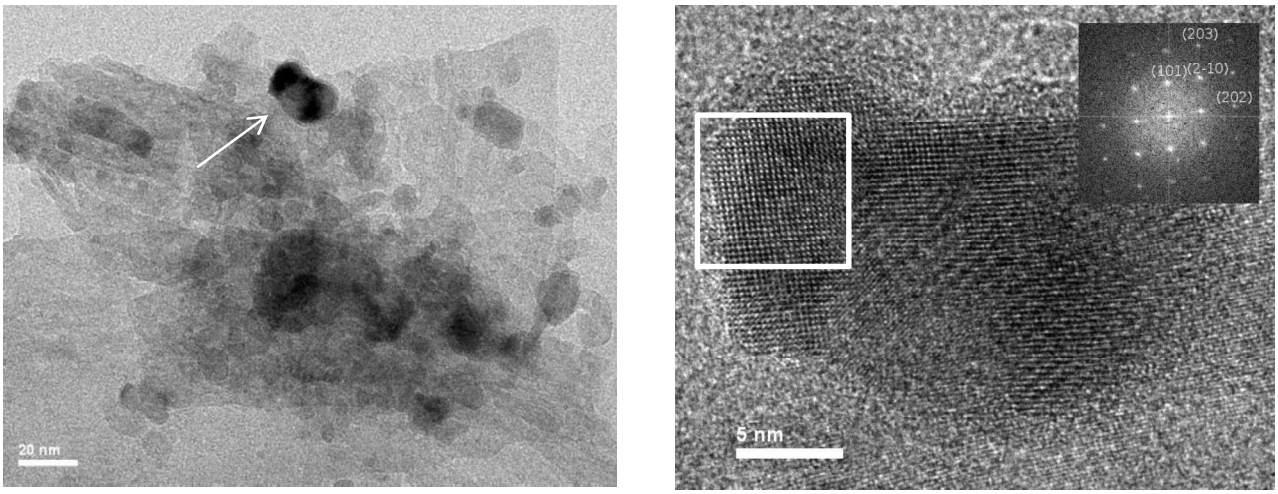

Figure 6 TEM images of NiS/γ-Al_2O_3 sample after a complete reaction with $AsPh_3$ ($AsPh_3$ initial concentration – 28.6 mmol.L^{-1}, As/Ni = 1, 230°C, 23 bar H_2). Left panel: low magnification general view. Right panel: high resolution image of the particle pointed by an arrow (insert – Fourier transform of the zone marked by white rectangle).

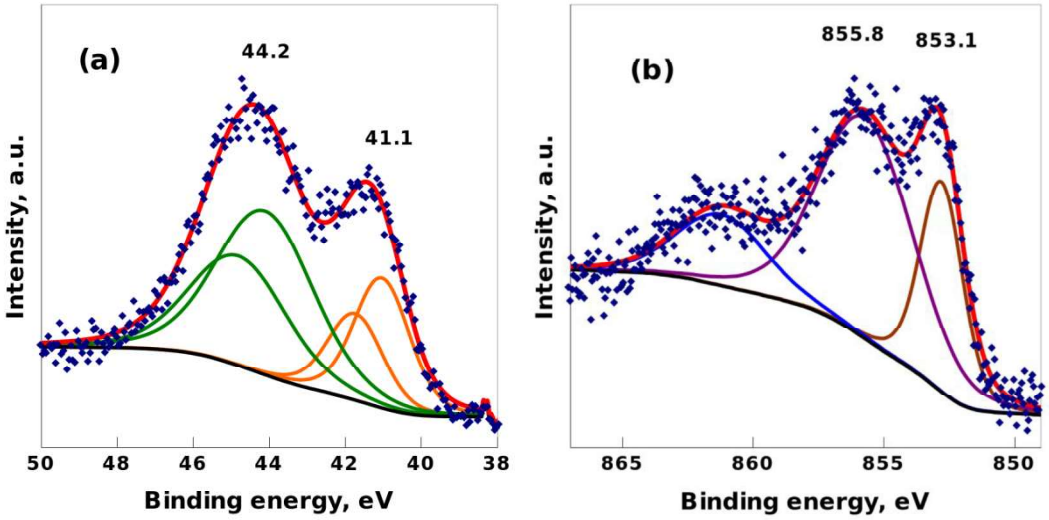

Figure 7 As 3d (a) and Ni $2p_{3/2}$ (b) narrow scan XPS spectra of NiS/γ-Al_2O_3 sample after reaction with $AsPh_3$ ($AsPh_3$ initial concentration – 28.6 mmol.L^{-1}, As/Ni = 1, 230°C, 23 bar H_2).

To complete the bulk techniques (XRD and HRTEM) the surface composition of the reacted sample

was analyzed using XPS. As 3d spectrum contains two peaks each corresponding to an unresolved doublet of $As3d_{3/2}$ and $As3d_{5/2}$ (Fig.7a). The position of the low energy peak (41.1 eV) corresponds to NiAs phase and the second peak, located at 44.2 eV, can be attributed to arsenite species [16]. Appearance of oxidized As on the surface of NiAs particles is due to a strong sensitivity of As to trace amount of oxygen. Thus, it was shown that As^{+3} was formed even on the surface of NiAs monocrystal cleaved in XPS chamber [16]. Given the small particle size of NiAs in our sample and less stringent conditions used for sample transfer to XPS chamber, the surface oxidation can hardly be avoided in our case. Ni 2p3/2 spectrum (Fig.7b) is similar to that observed in the initial sulfide sample (see Fig.3b). The peak at 853.1 eV is attributed to NiAs and the contribution at 855.8 eV is due to Ni^{2+} in oxygen environment (O or OH) [15,16]. The presence of oxygen in Ni surrounding can stem from incomplete reaction of NiO present in the sample and/or from a partial hydrolysis of NiAs during transfer to the XPS chamber.

3.3 Effect of Ni phase and of ligand in AsR_3 species on the reactivity

Despite a model character of our study, we tried to evaluate the role of two important parameters relevant to the industrial scale application of As trapping masses. First of them is the nature of the supported Ni-containing phase (Ni^0 and NiO) and second is the composition of the reacting As species.

The importance of the first parameter is related to the fact that Ni-based trapping masses used in the industrial practice sometimes are prepared by *in situ* sulfidation of supported Ni species. Under these conditions the sulfidation can be incomplete and along with Ni sulfides other Ni-containing species may be present in the sorbent. To compare their reactivity with that of NiS, we performed additional experiments with alumina-supported Ni^0 and NiO under the same conditions as for NiS (Fig.8). It follows that the chemical nature of Ni phase has a strong impact on the reactivity towards $AsPh_3$. Metallic Ni is the most reactive phase, while NiO shows only a very weak activity in $AsPh_3$ trapping. This difference can be attributed to a well-known strong hydorgenolysis activity of

metallic Ni [17]. Addition of non-metallic elements (S or P) on the Ni surface results in attenuation of this activity due to lowering of the electronic density on Ni atom and therefore weaker interaction with adsorbed species [18]. The trend observed in Fig.8 can be explained by the same phenomenon. Appearance of sulfur in Ni environment (in NiS) results in a slight lowering of reactivity in comparison with metallic Ni. Further decrease of electronic density on Ni atoms in NiO reduces dramatically its hydrogenolysis activity and therefore its reactivity in $AsPh_3$ decomposition.

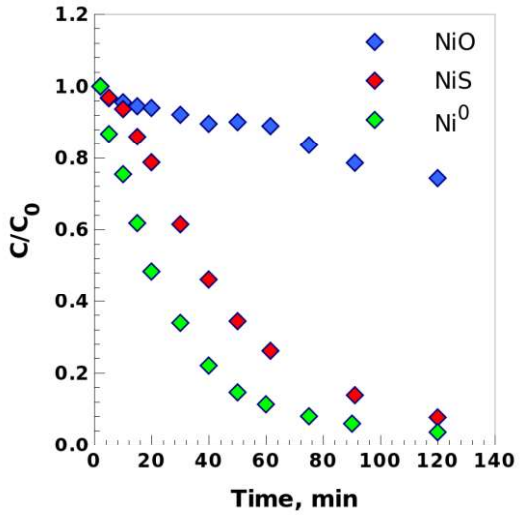

Figure 8 $AsPh_3$ conversion as a function of time for different Ni phases supported on γ-Al_2O_3 ($AsPh_3$ initial concentration – 28.6 mmol.L^{-1}, As/Ni = 1, 230°C, 23 bar H_2).

The dramatic drop of reactivity when going from NiS to NiO has an important practical implication. It suggests that for obtaining an active trapping mass the high sulfidation degree must be achieved in order to avoid the presence of residual NiO. This could be done, for example, using preferentially *ex situ* sulfidation under high H_2S concentration instead of *in situ* sulfidation procedure.

The second parameter, composition of As-containing species, is important since in the treated feedstocks various As-containing molecules were detected which contain different aliphatic and aromatic ligands [19]. It would be useful therefore to evaluate the impact of composition of As species on their decomposition rate. To do so we studied under similar conditions the trapping of triethyarsine ($AsEt_3$). The obtained conversion curves (Fig.9) show that at 230°C $AsEt_3$ is very difficult to decompose and only increase of temperature to 260°C allows to obtain a measurable

conversion. This dramatic difference of reactivity between $AsEt_3$ and $AsPh_3$ can be explained in terms of relative stability of -Et and -Ph ligands. The higher stability of - Ph intermediates in comparison with -Et ones (due to resonance effect) should facilitate As-C bond rupture in the case of $AsPh_3$ and make more rapid the overall reaction.

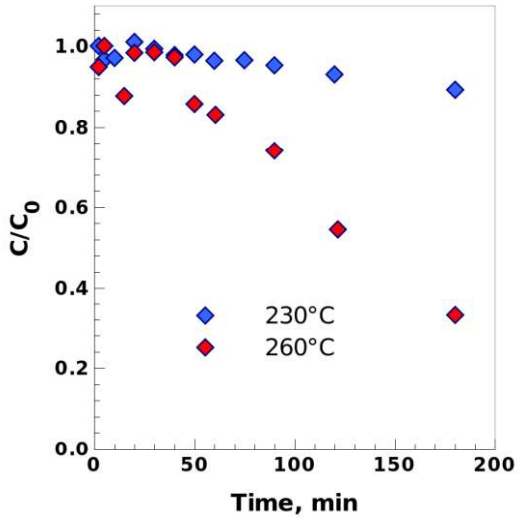

Figure 9 $AsEt_3$ conversion as a function of time in the reaction with NiS/γ-Al_2O_3 at 230 and 260°C ($AsEt_3$ initial concentration – 28.6 mmol.L^{-1}, As/Ni = 1, 23 bar H_2).

3.4 Role of the solid phase diffusion in $AsPh_3$ trapping

The analysis of the conversion curves of $AsPh_3$ for different As/Ni ratios shows that the decrease of concentration is linear at the beginning of the reaction, but becomes slower at the end (Fig.S3). This change means that at the beginning of the reaction the rate of reaction is constant but it declines when reaction proceeds. Such a decrease of the decomposition rate in a batch reactor can have one of two following reasons or their combination. First, it can be provoked by the decrease of the concentration of reacting species with time. Second, in our case it can be related to the formation of NiAs product layer creating a diffusion barrier for the reaction. Since these two effects occur simultaneously, the analysis of the standard conversion curves does not allow to distinguish which one is responsible for the decrease of the reaction rate.

To clarify this important point we performed additional experiments in which As/Ni ratio was equal

to 1, but $AsPh_3$ was added to the reactor in four successive doses. After injection of each dose we waited until a complete transformation of added $AsPh_3$ (~ 2 h) and then the next dose was injected (Fig.S4). The comparison of the obtained conversion curves shows that for three doses of $AsPh_3$ they are very close and only for the fourth dose the reaction rate declines (Fig.10). This finding shows that the presence of NiAs layer slows down the reaction only after the transformation of three injected doses which corresponds to conversion of ~ 50 % of Ni into NiAs. Below this value $AsPh_3$ transformation rate is not limited by diffusion through NiAs layer.

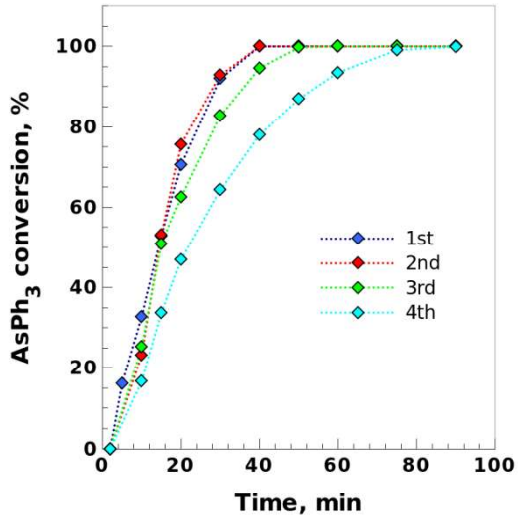

Figure 10 Conversion of $AsPh_3$ in the reaction with NiS/γ-Al_2O_3 as a function of time for successive injected doses (total As/Ni = 1, 230°C, 23 bar H_2). The lines are guides for the eyes.

The absence of diffusion limitations in solid transformation up to 50 % of conversion is a rather unexpected result. Its origin in our system can be understood using the shrinking core model of solid phase transformation [20]. For a spherical particle of initial radius R this model gives the following relationship between the product layer thickness (Δr) and the transformation degree:

$$\Delta r = R\left(1 - (1 - X)^{1/3}\right)$$

Using the values R = 4.5 nm (NiS average crystallite size is 9 nm, section 3.1) and X = 0.5 one can obtain that the thickness of the formed NiAs layer is about 0.9 nm. The obtained value is an estimation since some factors were not taken into account such as the size dispersion of NiS

crystallites or the presence of NiO phase. Nevertheless the obtained value suggests that even after conversion of 50 % of the active phase the product layer consists of very small crystallites. Due to this fact the formed NiAs layer should contain a large number of grain boundaries providing pathways for fast diffusion similarly to other solid state transformations [21].

If the diffusion through NiAs layer is not a rate determining step for conversion degree below ~ 50 %, the question arises about the nature of this step. Unfortunately, the batch reactor used in the present study does not allow a detailed kinetic analysis which can be applied for the measurements realized at the constant concentration [20]. However our data allow to formulate some hypotheses. Thus, the replacement of S by As on the surface (first step of NiS transformation), cannot represent the rate determining step since its rate should depend on the S/As ratio at the surface and therefore on the conversion degree. More generally, the fact the rate of $AsPh_3$ decomposition is independent of the sorbent conversion allows to suggest that the rate determining step does not involve solid modification. It should therefore be related to the transformation of the organic substrate - $AsPh_3$. Possibly it consists in As-C hydrogenolysis allowing to release As atoms which replace S atoms in NiS structure. We do not have direct evidence proving this hypothesis, but it is in line with the much lower reactivity of $AsEt_3$ (see section 3.3).

For conversion degrees higher than 50 % diffusion through NiAs layer starts to contribute to the slowdown of the reaction. In addition, NiO particles present in our sorbent react at high conversion, but at much lower rate than NiS (see section 3.3). The change of the reaction mechanism at ~ 50 % of conversion for the experiment with initial As/Ni=1 corroborates with a sharp decrease of the transformation rate observed after this value (see Fig. 4).

3.5 Mechanism of $AsPh_3$ decomposition on NiS

As we mentioned in section 3.2 the concentrations of the reaction products in the liquid phase vary with time in a complex manner (see Fig.4). While the concentration of benzene increases, those of thiophenol and diphenylsulfide pass through the maximum but not at the same time. In this section

we will sketch a possible mechanism of $AsPh_3$ decomposition allowing to explain these trends.

The first question concerns the possible relationship between the observed variation of the concentrations and the appearance of the diffusion limitations after 50 % of Ni conversion. For the experiment with the initial As/Ni = 1 such correlation seems to exist since the maximum of thiophenol concentration is indeed observed at ~ 50 % of $AsPh_3$ (and Ni) conversion (see Fig.4). However, during the test with the initial ratio As/Ni = 0.4 the trend for thiophenol is the same (Fig.11), but the maximum concentration is reached at ~ 40 min after decomposition of 73% of $AsPh_3$ which corresponds to conversion of 29 % of Ni. For the tests with As/Ni = 0.2 this value is even lower: the maximum in thiophenol concentration is observed after only ~ 15 % of Ni being transformed (Fig.S5). We conclude thus that the observed variation of the products concentration is not correlated with the changes in the sorbent composition. These trends should therefore be explained by interconversion of different species in H_2 atmosphere in the presence of $NiS/\gamma\text{-}Al_2O_3$.

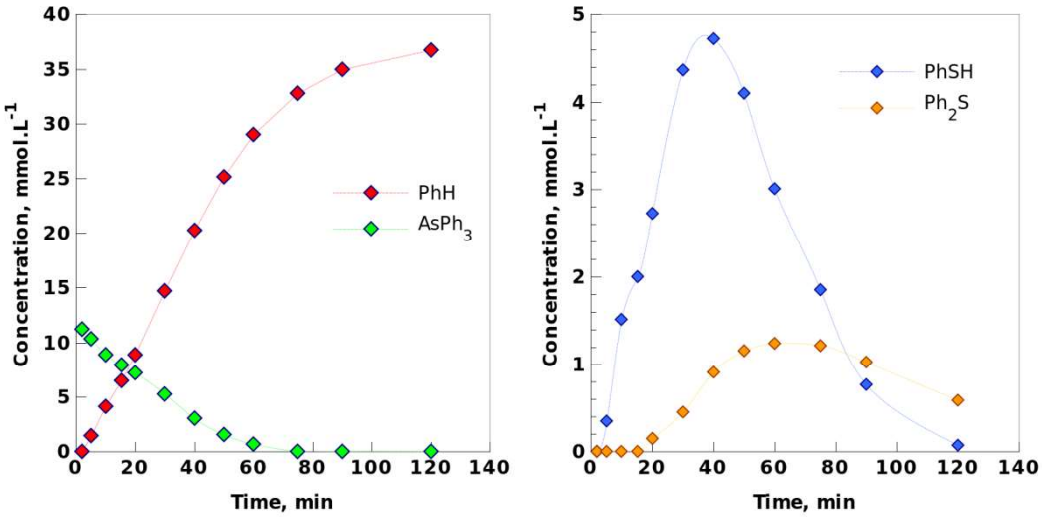

Figure 11 Time evolution of the concentrations of $AsPh_3$ and of the reaction products in the liquid phase during reaction of $AsPh_3$ with $NiS/\gamma\text{-}Al_2O_3$ (initial As/Ni ratio – 0.4, 230°C, 23 bar H_2). The lines are guides for the eyes.

In the following we will describe the possible processes taking place at different stages of the reaction between $AsPh_3$ and NiS. Our analysis is based on the data obtained for As/Ni=0.4 for two reasons. First, the concentrations of all products are sufficiently high to be measured accurately.

Second, in this case the amount of NiS in the sorbent is sufficient to capture all As and therefore the interaction with much less reactive NiO can be neglected.

The reaction can be divided in three distinct ranges (Fig.11). The first one extends from the beginning up to 40 min when the maximum of thiophenol concentration is achieved. Simultaneous formation of PhH and PhSH shows that the main reaction in this range is:

$NiS + AsPh_3 + 3/2H_2 \rightarrow NiAs + 2PhH + PhSH$ (1)

However, the ratio PhH/PhSH observed in this range (~ 3.3) is higher than that predicted by reaction (1). It means that another reaction producing only PhH occurs at the same time:

$NiS + AsPh_3 + 5/2H_2 \rightarrow NiAs + 3PhH + H_2S$ (2)

The absence of Ph_2S at the beginning of the reaction shows that it is a secondary reaction product forming possibly from PhSH when its concentration is sufficiently high:

$2PhSH \rightarrow Ph_2S + H_2S$ (3)

The second range is observed from 40 min to 75 min, the high limit corresponding to the disappearance of $AsPh_3$. The fact that the decrease of thiophenol concentration is accompanied by the increase of that of Ph_2S signifies that reaction (3) proceeds at this stage. In the same time benzene concentration continues to increase due to reaction (2) and also possibly via desulfurisation of PhSH and Ph_2S:

$PhSH + H_2 \rightarrow PhH + H_2S$ (4)

$Ph_2S + 2H_2 \rightarrow 2PhH + H_2S$ (5)

The occurrence of these reactions in our case is confirmed by the fact that after the complete transformation of $AsPh_3$ (75 – 120 min) the sulfur-containing species disappear and benzene concentration continues to rise (Fig.11). It is worth noting that reactions (4), (5) and possibly (3) need a catalyst to proceed under the used conditions. They occur therefore on the surface of the trapping mass and may thus compete with the reactions involved in $AsPh_3$ decomposition. Given the high concentration of formed PhSH (e.g. at 40 min it is higher than that of $AsPh_3$, Fig.11), these reactions can contribute to the slowing down of $AsPh_3$ decomposition at the high conversion

degrees.

3.6 Kinetic model of $AsPh_3$ decomposition

As detailed previously, the $AsPh_3$ conversion pattern follow the same trend for all As/Ni ratio, with a constant rate at the beginning of the experiment, and a decreasing rate at the end (Fig.S3). Thus, a simple kinetic model, using zero or first order with respect to $AsPh_3$, is not able to describe properly these conversion profiles. A partial order with respect to $AsPh_3$ should yield a better fit, however, it will not be able to describe correctly this peculiar pattern, corresponding to the change of the reaction order from zero to one.

Before discussing the kinetic model, the role of H_2 should be evaluated since it is involved in almost all mentioned reactions. To do so, we performed an additional test at 10 bar of H_2 instead of 23 bar used in all described experiments and we found that the conversion profiles are very similar (Fig.S6). This result shows that under high H_2 pressure, used in our study, the amount of active hydrogen species participating in the reaction is not a limiting factor whatever their exact nature. Therefore our model does not include H_2 pressure explicitly.

Taking into account the complex network of reactions involved in $AsPh_3$ decomposition, we can hardly apply the detailed classical kinetic models. We propose therefore a simplified kinetic model based on the reversible adsorption of $AsPh_3$ followed by its decomposition considered as a one-step reaction of the first order:

$$AsPh_3(liq) \overset{\frac{k_1}{k_{-1}}}{\leftrightarrow} AsPh_3(ads) \overset{k}{\rightarrow} Products$$

We assume that the rate determining step of reaction is the decomposition of adsorbed $AsPh_3$. In this case the surface reaction rate can be written in the following way:

$$r_S = -\frac{1}{S_{act}}\frac{dN(AsPh_3)}{dt} = -\frac{d[AsPh_3(ads)]}{dt} = k[AsPh_3(ads)] = k\theta N_M \quad \{1\}$$

Where r_S (mol·m^{-2}·s^{-1}) is the surface reaction rate, S_{act} (m^2) is the active surface area of the trapping mass, N($AsPh_3$) (mol) is the amount of transformed $AsPh_3$, k (s^{-1}) is the decomposition rate constant, [$AsPh_3$(ads)] (mol·m^{-2}) is the surface concentration of $AsPh_3$, θ is the surface fraction occupied by $AsPh_3$, N_m (mol·m^{-2}) is the $AsPh_3$ monolayer adsorption capacity.

Application of the steady state approximation to [$AsPh_3$(ads)] gives:

$$\frac{d[AsPh_3(ads)]}{dt} = 0 = k_1[AsPh_3](1-\theta)N_M - k_{-1}[AsPh_3(ads)] - k[AsPh_3(ads)] =$$

$$k_1[AsPh_3](1-\theta)N_M - k_{-1}\theta N_M - k\theta N_M \qquad \{2\}$$

Where [$AsPh_3$] (mol·m^{-3}) is the liquid phase concentration of $AsPh_3$, k_{-1} (s^{-1}) is the desorption rate constant and k_1 (m^3·mol^{-1}·s^{-1}) is the adsorption rate constant.

Using this equation the surface coverage θ can be determined:

$$\theta = \frac{k_1[AsPh_3]}{k_{-1} + k + k_1[AsPh_3]} \qquad \{3\}$$

The surface reaction rate can thus be expressed as:

$$r_S = k\theta N_M = \frac{K_1[AsPh_3]}{1 + K_2[AsPh_3]} \qquad \{4\}$$

with :

$$K_1 = kN_M\frac{k_1}{k_{-1}+k} \qquad K_2 = \frac{k_1}{k_{-1}+k}$$

To obtain the values of K_1 and K_2, the rate of the surface reaction must be related to the measured rate of $AsPh_3$ disappearance in the liquid phase (volume reaction rate). This relationship can be obtained using the fact that both the surface and the volume reaction rates correspond to the transformation of the same amount of $AsPh_3$:

$$r_V = -\frac{d[AsPh_3]}{dt} = -\frac{1}{V_{sol}}\frac{dN(AsPh_3)}{dt} = \frac{S_{act}}{V_{sol}}\ r_S = Ar_S \qquad \{5\}$$

Where r_V (mol·m^{-3}·s^{-1}) is the volume reaction rate, V_{sol} (m^3) is the volume of solution. It follows from equation {5} that the rate of reaction measured in solution is proportional to the rate of the surface reaction. Unfortunately the value of the proportionality coefficient cannot be calculated since the active surface area (S_{act}) is not known. Combination of equations {4} and {5} results in the following expression for disappearance rate of $AsPh_3$ in solution:

$$r_V = -\frac{d[AsPh_3]}{dt} = \frac{AK_1[AsPh_3]}{1 + K_2[AsPh_3]} = \frac{K_1'[AsPh_3]}{1 + K_2[AsPh_3]} \qquad \{6\}$$

Where K_1' (s^{-1}) is the new constant which includes the proportionality coefficient A.

With such equation, the reaction order depends on the concentration of $AsPh_3$ in the liquid phase: at high concentration (at the beginning of the reaction) the reaction order is zero ($r \sim K_1'/K_2$), whereas at the end of the reaction, the order is one ($r \sim K_1'\ [AsPh_3]$). Table 2 gives the optimized values of K_1' and K_2 which allow the best fit of the data for the different experiments and Fig.12 compares the experimental data with the optimized model fits. It can be concluded that similar values of K_1' and K_2 are obtained for the experiments where As/Ni ratio is smaller than one. In contrast for the experiment where As/Ni = 1, the constants are one order of magnitude lower, which may be due to appearance of other phenomena which slow down the reaction. As detailed previously, for As/Ni ratio higher than 0.5 diffusion through formed NiAs layer becomes slower and might decrease the overall reaction rate. Also, the presence of less reactive NiO can play the same role.

Table 2 Constants of equation {6} obtained from the fit of the experimental conversion profiles for different As/Ni initial ratios

As/Ni initial molar ratio	$K_1' \cdot 10^3$ **(s^{-1})**	K_2 **(L.mmol^{-1})**
1	0.43	0.012
0.4	3.0	0.75
0.2	2.3	0.75
0.1	2.4	0.85
0.05	3.2	0.80

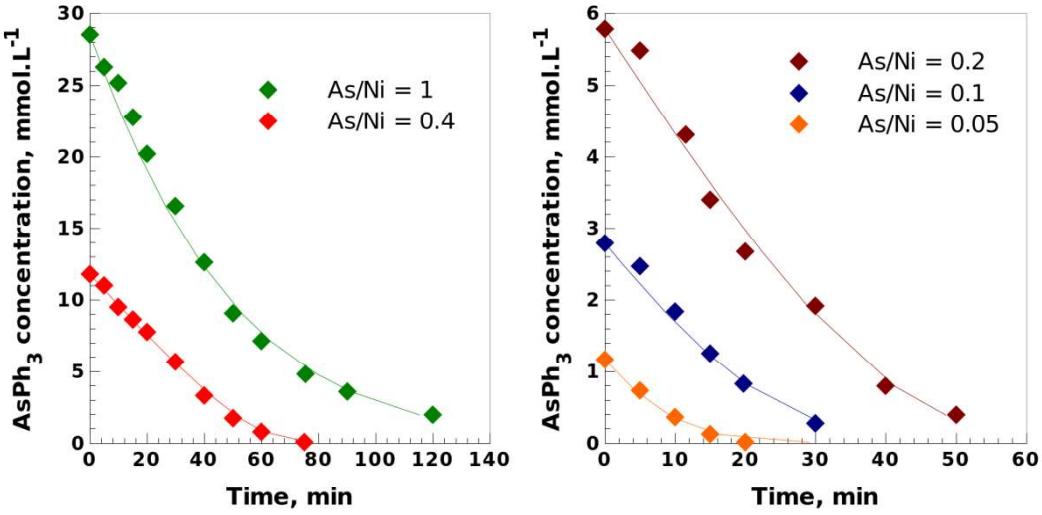

Figure 12 $AsPh_3$ conversion profiles for different initial As/Ni ratio (230°C, 23 bar H_2). Points are the experimental data, lines are the fits with equation {6} using the parameters given in Table 2.

4. Conclusions

In the context of trapping of As-containing species in petroleum feedstocks we studied reaction between $AsPh_3$ and NiS/Al_2O_3. The rate of disappearance of $AsPh_3$ was measured in a batch reactor in toluene solution at 230°C under 23 bar of H_2. The experiments were performed for different $AsPh_3$ concentrations (1.1 – 28.6 $mmol.L^{-1}$) and constant $NiS/\gamma\text{-}Al_2O_3$ amount corresponding to variation of As/Ni ratio in the range 0.05 - 1. These kinetic measurements and additional experiments allowed to determine the following main features of the reaction mechanism:

- The end reaction products are: NiAs, benzene and H_2S. The intermediate products, thiophenol and diphenylsulfide, were also observed in the liquid phase during reaction.
- For Ni conversion below ~ 50 % the diffusion through formed NiAs layer is not the rate determining step. Under these conditions the hydrogenolysis of C-As bonds appears to be the rate determining step.
- The decomposition of $AsPh_3$ follows the conversion profile with the rate order changing from zero at the beginning of reaction to one at the end. This trend is successfully described by a proposed kinetic model based on the decomposition of adsorbed $AsPh_3$.

- The reactivity of NiO towards $AsPh_3$ is much lower than that of NiS. This fact highlights the importance of a complete sulfidation of As trapping masses.

An important general point revealed by our study concerns the fact that a stoichiometric NiS – NiAs transformation involves a key catalytic step. The decomposition of As molecular species (producing As atoms) occurs through their heterogeneous catalytic reaction with H_2. Moreover, at low conversion this catalytic reaction becomes a rate determining step which results in a strong difference in reactivities of NiS towards $AsPh_3$ and $AsEt_3$. The presence of this catalytic step explains also a much lower reactivity of NiO in comparison with NiS.

Acknowledgments

We thank Remi Chassagnon and Olivier Heintz (Laboratoire Interdisciplinaire Carnot de Bourgogne) for performing HRTEM and XPS measurements.

References

1. J.B. Stigter, H.P.M. de Haan, R. Guicherit, C.P.A. Dekkers, M.L. Daane, Environ. Pollut. 107 (2000) 451.

2. A. de Jesus, A.V. Zmozinski, I.C.F. Damin, M.M. Silva, M.G.R. Vale, Spectrochim. Acta B 66 (2012) 86.

3. B. Bouyssiere, F. Baco, L. Savary, H. Garraud, D. L. Gallupe, R. Lobinski, J. Anal. At. Spectrom. 16 (2001) 1329.

4. M. D. Argyle, C. H. Bartholomew, Catalysts 5 (2015) 145.

5. B. Nielsen, J. Villadsen, Appl. Catal. 11 (1984) 123.

6. R. N. Merryfield, L. E. Gardner, G. D. Parks, in: M. L. Deviney, J. L. Gland (Eds.), Catalyst Characterization Science, ACS Symposium Series, 1985, p.2-14.

7. A. Puig-Molina, L. P. Nielsen, A. M. Molenbroek, K. Herbst, Catal. Lett. 92 (2004) 29.

8. S. Yang, J. Adjaye, W. C. McCaffrey, A. E. Nelson, J. Mol. Catal. A: Chem. 321 (2010) 83.

9. Picard, F; Coupard, V.; Bouchy, C. French Patent FR2876113 B1 (2008).

10. B. Didillon, L. Savary, Y. A. Ryndin, J.-P. Candy, J.-M. Basset, C. R. Acad. Sci. Paris, Serie IIc, Chimie: Chemistry 3 (2000) 413.

11. Y. A. Ryndin, J.-P. Candy, B. Didillon, L. Savary, J.-M. Basset, C. R. Acad. Sci. Paris, Serie IIc, Chimie : Chemistry 3 (2000) 423.

12. Y. A. Ryndin, J.-P. Candy, B. Didillon, L. Savary, J.-M. Basset, J. Catal. 198 (2001) 103.

13. V. Maurice, Y. A. Ryndin, G. Bergeret, L. Savary, J.-P. Candy, J.-M. Basset, J. Catal. 204 (2001) 192.

14. Y. A. Ryndin, J.-P. Candy, G. Bergeret, L. Savary, D. Uzio, J.-M. Basset, Stud. Surf. Sci. Catal. 139 (2001) 479.

15. D.L. Legrand, H.W. Nesbitt, G.M. Bancroft, American Mineralogist 83 (1998) 1256.

16. H. W. Nesbitt, M. Reinke, American Mineralogist 84 (1999) 639.

17. G. Leclercq, L. Leclercq, L. Bouleau, S. Pietrzyk, R. Maurel, J. Catal. 88 (1984) 8.

18. G. Wang, S. Zhang, X. Zhu, C. Li, H. Shan J. Ind. Eng. Chem. 86 (2020) 1.

19. P. Sarrazin, C. J. Cameron, Y. Barthel, M. E. Morrison, Oil and Gas Journal 91 (1993) 86.

20. J. Szekely, J.W. Evans, H.Y. Sohn, Gas-Solid Reactions, Academic Press, New York,1976.

21. J. Skrzypski, I. Bezverkhyy, O. Heintz, J.-P. Bellat, Ind. Eng. Chem. Res. 50 (2011) 5714.

Trapping $AsPh_3$ via reaction with $NiS/\gamma\text{-}Al_2O_3$ in the presence of H_2: reaction mechanism and kinetics

Angélique Jallais,[a] Michel Thomas,[a] Antoine Hugon,[a] Igor Bezverkhyy[b*]

[a] IFP Energies nouvelles, Rond-point de l'échangeur de Solaize, BP 3, 69360, Solaize, France

[b] Laboratoire Interdisciplinaire Carnot de Bourgogne, UMR 6303 CNRS-Université de Bourgogne Franche-Comté, BP 47870, 21078 Dijon Cedex, France

*Corresponding author

Abstract

Removal of As from petroleum feedstocks is an important process which can be realized using As trapping mass containing supported nickel sulfide. In order to understand the mechanism of the trapping we studied the reaction of $AsPh_3$ with $NiS/\gamma\text{-}Al_2O_3$ in the presence of H_2 in a batch reactor in toluene solution at 230°C. This reaction results in formation of NiAs, benzene and H2S. Also, the intermediate species, thiophenol and diphenylsulfide, were observed. Despite formation of NiAs layer in the course of reaction, the rate of $AsPh_3$ decomposition is not affected by the solid state diffusion up to ~ 50% of nickel conversion. The rate determining step in these conditions appears to be the hydrogenolysis of As-C bonds. It was found that the reaction order changes in the course of reaction from zero to one. This trend is described by a kinetic model assuming adsorption of $AsPh_3$ molecules followed by decomposition.

Keywords: As trapping mass, protection of hydrotreatment catalysts, dearsenification

1. Introduction

Arsenic can be naturally found in crude oils at very low concentrations, often comprised between 10 and 200 $\mu g.kg^{-1}$ (10-200 ppb) [1,2] as determined by graphite furnace atomic absorption spectrometry (GF-AAS). It can also be found in distillation cuts, gas condensates [3] or feed streams treated in catalytic processes, mainly as organic arsenic compounds AsR_3.

It is known that organic arsenic can be a severe poison for different types of catalysts [4]. It has been shown that arsenic can poison nickel steam reforming catalysts forming NiAs or Ni_5As_2 as a final phase [5]. It has also been proved that As is a strong poison of hydrotreating catalyst such as sulfided $CoMo/Al_2O_3$ [6] which is used to decrease the S content below 10 ppm of FCC gasoline in order to meet commercial specifications.

Two studies have been realized to understand the mechanism of As poisoning in hydrotreating catalysts [7-8]. A deactivated $NiMoP/Al_2O_3$ hydrotreating catalyst was characterized by EXAFS in the work of Puig-Molina et al. [7]. The studied material was exposed to few ppb levels of As for several years in an industrial reactor and was resulfided before the EXAFS measurements. It was concluded about the possible formation of As_2S_3 but the formation of As-Ni bonds was not observed. Also, the authors suggest that the deactivation of the catalyst by As could be explained by the formation of Ni-S-As bounds leading to the blockage of Ni sites.

Nelson et al. [8] studied the arsenic poisining of NiMoS catalyst by DFT. It has been shown that As-containing molecules (AsH_3, trimethylarsine (TMA), triethylarsine (TEA), triphenylarsine (TPA)) can be adsorbed through the As atom onto the catalyst Ni atoms. The dissociation of arsenic compounds on NiMoS surface was studied and it was shown that the dissociation energy increases in the order AsH_3 < TPA < TEA < TMA, indicating a strong influence of the ligand nature on the reactivity of arsenic species. This study also showed that As atoms can be incorporated into the NiMoS catalyst through substitution of Ni or S atoms.

In order to protect HDS catalysts from poisoning by As, arsenic trapping masses have been developed which are based on nickel deposited on alumina [9]. They may be placed either in a separate guard bed upstream the HDT unit or in the same bed as the catalyst close to the entry of the feed. In this case, the operating conditions (temperature, hydrogen pressure, residence time) are fixed by the catalytic section. The trapping mass can be sulfided either prior to use or in situ by traces of H_2S or sulfur-containing molecules present in the feed.

The information about the mechanism of As trapping by these masses is very scarce. Only the reaction between Ni^0 and TPA in H_2 atmosphere has been studied by Ryndin et al. in a series of works [10-14]. It has been found that after a sufficient time of contact the metallic nickel was completely transformed into a single phase of NiAs (nickeline) and the mechanism for this reaction has been proposed. It proceeds through TPA adsorption on the surface sites followed by the hydrogenolysis of the As-C bounds with the formation of benzene and cyclohexane. Finally, migration of the As atom into the bulk of Ni^0 particles produces NiAs. Despite the importance of these results, they are not relevant to industrially used As trapping masses, since these materials contain Ni in sulfided and not in metallic form. In order to get a better understanding of the mechanism of As trapping by nickel sulfide, we studied in the present work the reactivity of NiS supported on alumina towards As-containing species.

Given a variety of As species present in different petroleum cuts, the choice of the representative species is not straightforward. We decided to study the reactivity of triphenylarsine (TPA or $AsPh_3$) as in the previous works [10-14]. Although the boiling temperature of this compound (360 °C) exceeds that of FCC gasoline (50-220°C), we chose TPA for two reasons. First, it is commercially available in a highly pure form and due to its low volatility it can be easily handled. Second, its use permits direct comparison of our results with those obtained for metallic nickel. To evaluate the effect of ligands on the reactivity we performed some additional experiments using triethylarsine ($AsEt_3$, TEA, T_{nbp} = 140 °C) under similar reaction conditions.

2. Experimental

2.1. Synthesis of NiS/γ-Al_2O_3 trapping mass

A mesoporous γ-Al_2O_3 in the form of extrudates with a surface area of 270 m^2/g was used as the support for the synthesis (the material was kindly provided by Axens, France). The NiO/Al_2O_3 precursor was prepared by the incipient wetness impregnation method using $Ni(NO_3)_2.6H_2O$ as nickel source (Alfa Aesar, 99.9985%). An amount of 20.81 g of nickel nitrate was dissolved in 15 mL of water then slowly dropped onto 25.80 g of dried alumina in a rotating beaker in order to soak the entire solid. It was then stored 24 hours under wet atmosphere to allow the diffusion of the nickel species into the alumina porosity and dried overnight in an oven at 100 °C. The calcination step was then performed at 450 °C for 2 hours under air.

A sample of NiO/Al_2O_3 was kept at this point and another was reduced under H_2 in order to obtain Ni^0/Al_2O_3. The rest of the NiO/Al_2O_3 was then sulfided under a flowing mixture of H_2S/H_2 (15 % v/v, Air Products) at 200 °C for 2 hours, at 350 °C for 1 hour and at 200 °C for 2 hours under H_2 only in order to remove the excess of sulfur. The sulfided solids were kept under argon.

2.2 Test of $AsPh_3$ trapping

The chemicals used in the study were obtained from the following providers: triphenylarsine (Sigma Aldrich, 97 %), triethylarsine (Strem chemicals, 98%), toluene (VWR chemicals, 99.8 %).

The reaction of triphenylarsine (TPA) with the synthesized trapping masses was carried out in a batch reactor, stirred by a mechanical agitator, in 250 mL of toluene, at 230 °C and under hydrogen pressure of 23 bar. Prior to the test, the desired amount of trapping mass was placed into the reactor under argon atmosphere, covered with toluene, and then the reactor was purged and pressurized with H_2. The temperature and the pressure of the reactor were established at the desired values and a known amount of TPA in toluene was introduced into the reactor using a connected charge vessel, pressurized with H_2 as well. A scheme of the unit can be seen in Fig.1.

In order to find conditions free of kinetic limitations due to internal and external mass transfer, the

experiments have been realized with different particle size in the range 0.4 – 3 mm. We have found that no limitations exist for particles smaller than 800 μm, therefore the particle fraction between 600 and 800 μm was used in the present study. Also, it was verified that the rate of reaction did not depend on the stirring rate, fixed at 1000 rpm. In addition to these experiments, the blank measurements were performed which showed that pure γ-Al_2O_3 is not active in $AsPh_3$ transformation in the used operation conditions (Fig.S1).

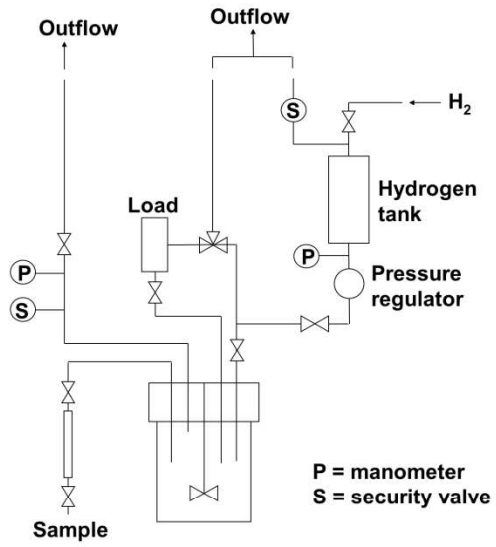

Figure 1 Scheme of the experimental setup used for the tests of $AsPh_3$ trapping in a batch reactor in H_2 atmosphere (see text for details).

The concentrations of TPA and of the reaction products in the solution were analyzed at regular intervals of time by gas-phase chromatographic analysis using an apparatus from Agilent. Injection was performed at 150°C with an injection volume of 0.2 μL. The column used for the separation was an Agilent DB-5 (30m x 0.32mm x 0.25μm) and detection was performed with a flame ionization detector (FID). Additional experiments were performed under different conditions in order to determine the relative standard errors of the concentration measurements. The following values were obtained: 6 % for triphenylarsine, 15 % for thiophenol (PhSH), 12 % for diphenylsilfide (Ph_2S) and 6 % for thriethylarsine ($AsEt_3$).

2.3 Characterization techniques

The XRD measurements were performed using a Panalytical X'Pert Pro diffractometer with a

Bragg-Brentano geometry using nickel-filtered Cu-Kα radiation (λ = 0.15406). In order to avoid any oxidation of the solids after the test, the samples were prepared in a glovebox under argon and the XRD cells were sealed with Kapton tape. For *in situ* XRD measurements during the sulfidation step the XRK 900 chamber from Anton Paar has been used. The protocol included a first step under a flowing mixture of H_2S/H_2 (15 % v/v) at 200 °C for 2 hours, then at 350 °C for 1 hour and finally at 200 °C for 2 hours under H_2 flow. Two measurements were done at each step of the sulfidation. The XRF measurements of the liquids and solids were performed using two wavelength dispersive X-ray fluorescence spectrometers, from Panalytical and Thermo Fisher Scientific. X-ray Photoelectron spectroscopy (XPS) was applied in order to determine surface composition of samples using the apparatus PHI 5000 Versaprobe with monochromatic Al Kα1 radiation. The samples were transferred to the XPS chamber under inert atmosphere. Transmission electron microscope images were recorded on a transmission electron microscope JEOL JEM-2100 under an accelerating voltage of 200 kV.

3. Results and discussion

3.1 Properties of the trapping mass

Considering the air sensitivity of the solids, determination of the nickel loading was performed before the sulfidation step using X-ray fluorescence. An average value of 13.8 Ni % (w/w) was determined for the different batches of the prepared trapping mass. The dispersion of Ni^0 (surface nickel atoms per total nickel atoms) was also measured using hydrogen chemisorption after reduction (410 °C for 16 hours then under vacuum at 350 °C for 3 hours). Assuming the stoichiometry of one chemisorbed hydrogen atom per surface nickel atom, a dispersion of 13 % was obtained.

To determine the crystalline phases formed during the synthesis the solids were analyzed by *in situ* XRD during the sulfidation step. As shown in Fig.2, after 2 hours at 350 °C under a flowing mixture of H_2S/H_2 (15% v/v), the observed phases are NiS (NiAs type) and γ-Al_2O_3. Applying the Debye-Scherrer equation to (2-10) diffraction peak of NiS (2θ = 53°) we found that the size of NiS

crystallites is 9 ± 0.9 nm. TEM was also applied to characterize the microstructure of the sample (Fig.S2). NiS particles can be distinguished on the images as darker regions, but unfortunately due to a poor contrast between NiS and γ-Al_2O_3 a detailed analysis of particle shape and size distribution was not possible.

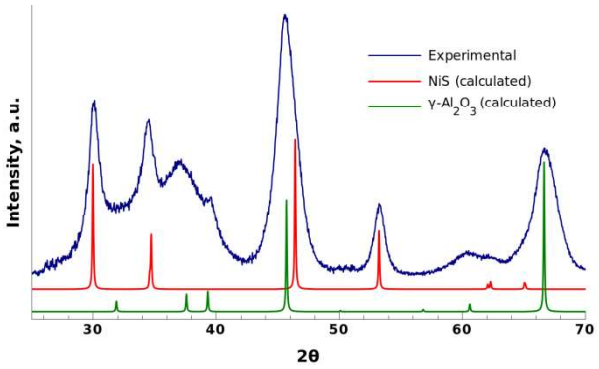

Figure 2 *In situ* XRD pattern of NiS/γ-Al_2O_3 sample used in the work.

The solids were analyzed by XRF in order to determine the mass percentage of nickel and sulfur. The results were 13.3 % for nickel and 5.7 % for sulfur which gives a S/Ni molar ratio of 0.8. Since the only observed Ni-S phase is NiS (NiAs type), this result suggests that part of the nickel oxide is not transformed during the sulfo-reduction step and that the NiS phase coexists with the remaining nickel oxide.

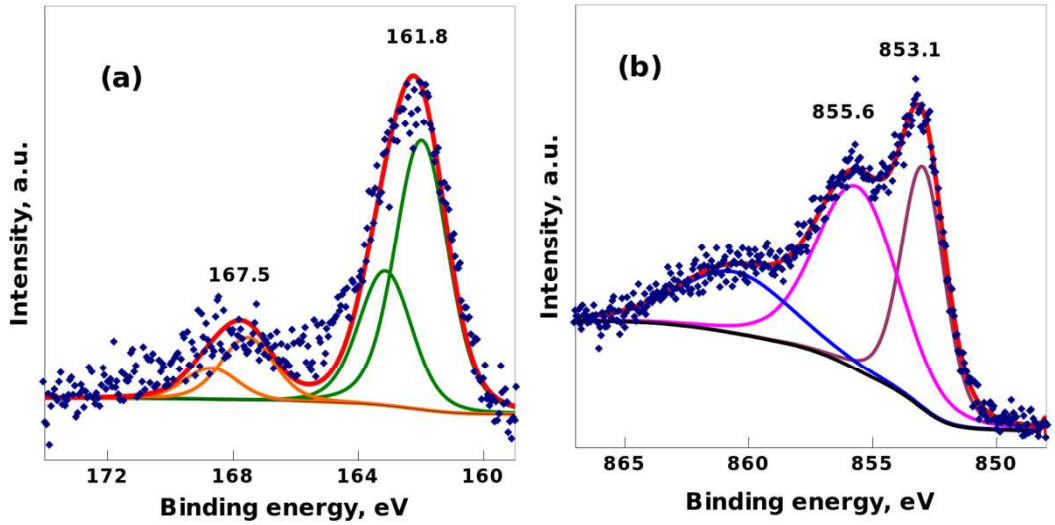

Figure 3 S 2p (a) and Ni $2p_{3/2}$ (b) narrow scan XPS spectra of NiS/γ-Al_2O_3 sample used in the work.

XPS results are in line with the XRD pattern and elemental analysis (Fig.3). S2p spectrum can be described by a sum of two unresolved doublets consisting of $S2p_{1/2}$ and $S2p_{3/2}$ peaks. The position of the main $S2p_{3/2}$ peak (161.8 eV) corresponds to S^{2-} in NiS [15]. A low intensity peak at 167.5 eV can be attributed to sulphate species formed after contact with trace amount of oxygen. Ni $2p_{3/2}$ spectrum can be described by a sum of two peaks with binding energies of 853.1 eV and 855.6 eV (a low intensity peak at ~ 861 eV corresponds to a satellite). The low energy component corresponds to Ni atoms in sulfur environment and the high energy one is characteristic of Ni^{2+} oxo or hydroxo species [15,16]. The presence of Ni-O species in XPS spectra and the value of the obtained atomic S/Ni ratio (0.75) confirm the presence of NiO in our sulfide sample.

3.2. Characterization of the products obtained after $AsPh_3$ trapping

The main reaction product in the liquid phase is benzene which represents more than 95 % of the species produced in the liquid phase after a complete decomposition of $AsPh_3$. Two intermediate species were also detected in the course of reaction: thiophenol (PhSH) and diphenylsulfide (Ph_2S) (Fig.4). Using these products yields the carbon balance close to 100 % suggesting that no other organic species were formed in significant concentration.

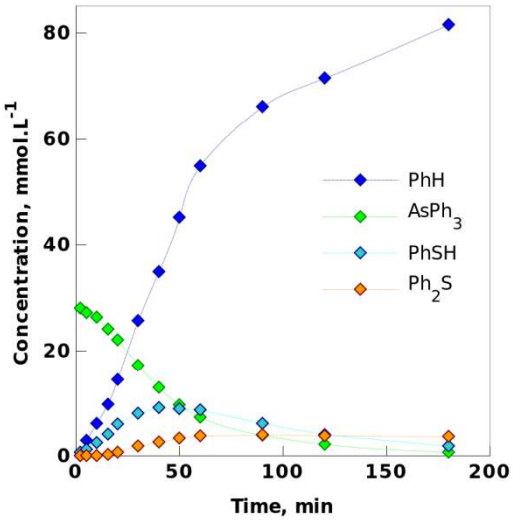

Figure 4 Concentration of the reaction products in the liquid phase as a function of time during reaction of $AsPh_3$ with NiS/γ-Al_2O_3 (As/Ni initial ratio – 1, 230°C, 23 bar H_2). The lines are guides for the eyes.

In contrast to solid products, the composition of the liquid phase could be measured as a function of time revealing different trends for the detected species. While the amount of benzene increases with time, the trends for the other products are more complex (Fig.4). The concentration of thiophenol passes through the maximum and that of diphenylsulfide achieves a plateau after certain time. For the experiment with As/Ni = 1 the time course of all products changes after ~ 50 min of reaction corresponding to decomposition of ~ 50% of the initial amount of $AsPh_3$. The origin of this change will be discussed in detail in section 3.5.

The sulfur content of the spent sorbent decreases when As/Ni ratio rises due to substitution of sulfur in NiS by arsenic during reaction (Table 1). However, the sulfur content of the liquid and solid phases does not correspond to the initial sulfur amount in the sorbent (Table 1). This effect can be due to formation of gaseous sulfur-containing species. Unfortunately the configuration of our test setup does not allow a quantitative analysis of the gas phase. Nevertheless, a gas sample was collected and analyzed using the gas chromatograph equipped with a sulfur specific FPD detector and the presence of H_2S was qualitatively confirmed.

Table 1 As and S concentrations in liquid and solid phases after the end of the test for different initial concentrations of $AsPh_3$

Concentration of $AsPh_3$		As/Ni initial molar ratio	Initial As amount, mmol	As, mmol		As balance	Initial S amount mmol (in NiS/Al_2O_3)			S balance
mmol/L	ppmw(As)			solid	liquid			solid	liquid	
28.6	2500	1	7.2	6.1	0.8	0.96	5.5	1.1	1.94	0.55
11.4	1000	0.4	2.9	2.7	nd	0.93	5.5	2.8	0.22	0.54
5.7	500	0.2	1.4	1.4	nd	1.0	5.5	3.6	nd	0.66
2.9	250	0.1	0.7	0.7	nd	1.0	5.5	4.6	nd	0.84
1.1	100	0.04	0.3	0.3	nd	1.0	5.5	5.1	nd	0.93

nd – not detected

In contrast to sulfur, the arsenic balance is close to unity (Table 1) evidencing that the reaction does

not produce any gaseous As species. Moreover, except at the highest used concentration, no As-containing species were found in the liquid phase. This finding shows that for the concentrations below 1000 ppm all the arsenic initially present in the solution is trapped on the sorbent. This observation is important from the application point of view. It means that in the industrially relevant concentration range (< 1 ppm) the use of NiS/Al_2O_3 could allow to trap all present arsenic on the solid sorbent without producing any gaseous or liquid phase As species.

To determine the nature of As-containing phase, we characterized by XRD the spent sorbent after reaction at the highest $AsPh_3$ concentration (Fig.5). The only arsenide phase detected in the pattern is NiAs (nickeline) whose crystallite size (9±1 nm) is very close to that of the initial NiS. For the trapping masses used in the tests with lower $AsPh_3$ concentrations the peaks of NiAs were not detected in the XRD patterns. This observation can be explained by the low amount of NiAs in these cases and/or by the small size of the crystallites in the partially converted samples.

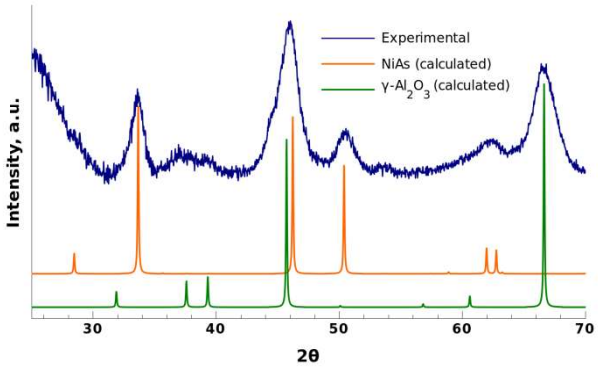

Figure 5 XRD pattern of $NiS/\gamma\text{-}Al_2O_3$ sample after a complete reaction with $AsPh_3$ ($AsPh_3$ initial concentration – 28.6 $mmol.L^{-1}$, As/Ni = 1, 230°C, 23 bar H_2).

In order to better describe the microstructure of the formed NiAs phase, the sample obtained after reaction was characterized by TEM (Fig.6, left panel). The typical low resolution image shows that the size of the formed NiAs particles varies in a wide range, from ~ 2 nm to more than 20 nm. The high resolution image of a large particle pointed by an arrow (Fig.6, right panel) shows the origin of this variability. The larger particles are polycrystalline consisting of smaller crystallites whose size is closer to that determined by XRD. The Fourier transform of the high resolution image shows the

presence of the lattice planes families with the distances characteristic of NiAs: 2.66 Å (101), 1.81 Å (2-10), 1.33 Å (202) and 1.14 Å (203). This fact confirms unambiguously our conclusion about formation of NiAs based on XRD.

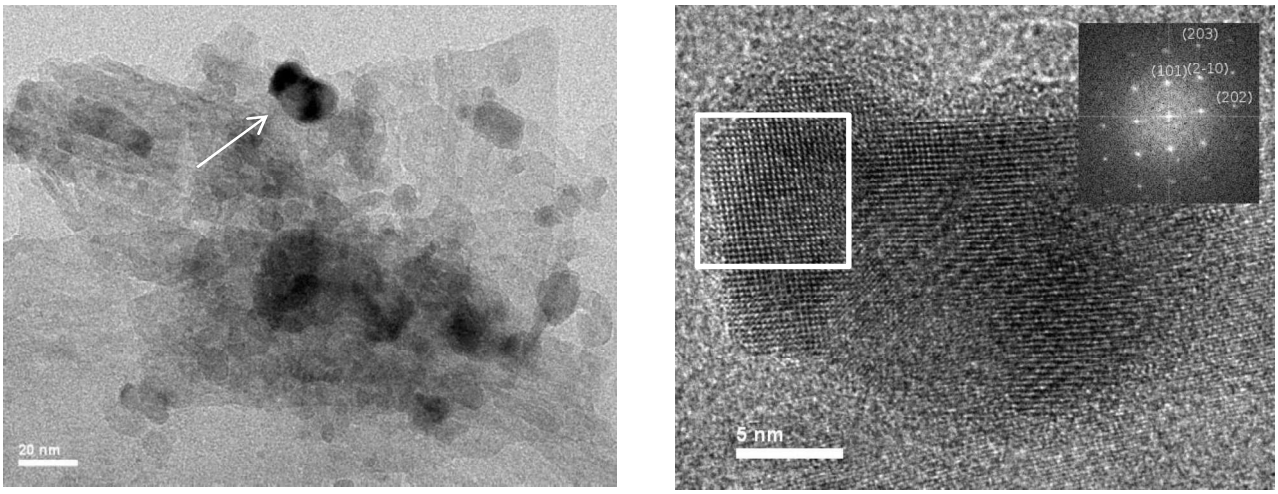

Figure 6 TEM images of NiS/γ-Al_2O_3 sample after a complete reaction with $AsPh_3$ ($AsPh_3$ initial concentration – 28.6 mmol.L^{-1}, As/Ni = 1, 230°C, 23 bar H_2). Left panel: low magnification general view. Right panel: high resolution image of the particle pointed by an arrow (insert – Fourier transform of the zone marked by white rectangle).

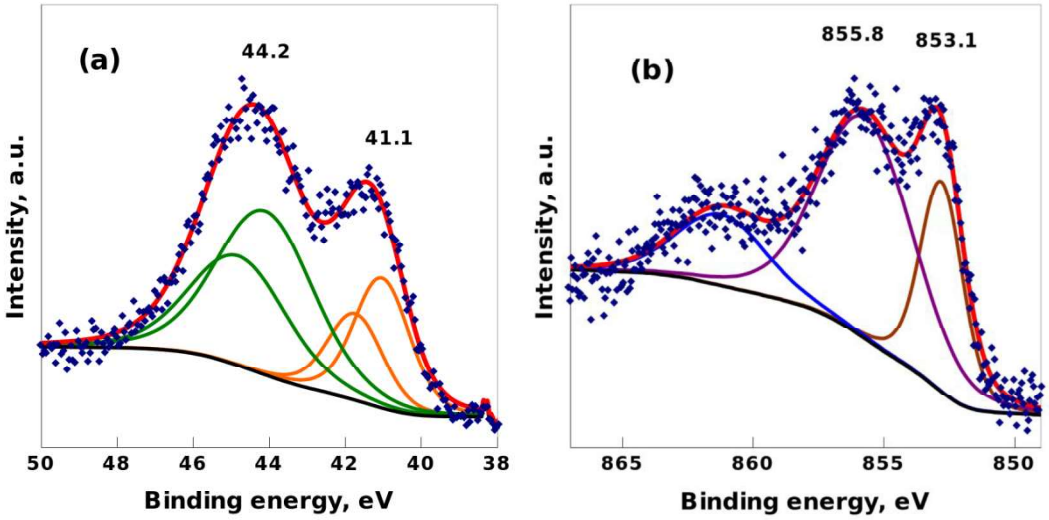

Figure 7 As 3d (a) and Ni $2p_{3/2}$ (b) narrow scan XPS spectra of NiS/γ-Al_2O_3 sample after reaction with $AsPh_3$ ($AsPh_3$ initial concentration – 28.6 mmol.L^{-1}, As/Ni = 1, 230°C, 23 bar H_2).

To complete the bulk techniques (XRD and HRTEM) the surface composition of the reacted sample

was analyzed using XPS. As 3d spectrum contains two peaks each corresponding to an unresolved doublet of $As3d_{3/2}$ and $As3d_{5/2}$ (Fig.7a). The position of the low energy peak (41.1 eV) corresponds to NiAs phase and the second peak, located at 44.2 eV, can be attributed to arsenite species [16]. Appearance of oxidized As on the surface of NiAs particles is due to a strong sensitivity of As to trace amount of oxygen. Thus, it was shown that As^{+3} was formed even on the surface of NiAs monocrystal cleaved in XPS chamber [16]. Given the small particle size of NiAs in our sample and less stringent conditions used for sample transfer to XPS chamber, the surface oxidation can hardly be avoided in our case. Ni 2p3/2 spectrum (Fig.7b) is similar to that observed in the initial sulfide sample (see Fig.3b). The peak at 853.1 eV is attributed to NiAs and the contribution at 855.8 eV is due to Ni^{2+} in oxygen environment (O or OH) [15,16]. The presence of oxygen in Ni surrounding can stem from incomplete reaction of NiO present in the sample and/or from a partial hydrolysis of NiAs during transfer to the XPS chamber.

3.3 Effect of Ni phase and of ligand in AsR_3 species on the reactivity

Despite a model character of our study, we tried to evaluate the role of two important parameters relevant to the industrial scale application of As trapping masses. First of them is the nature of the supported Ni-containing phase (Ni^0 and NiO) and second is the composition of the reacting As species.

The importance of the first parameter is related to the fact that Ni-based trapping masses used in the industrial practice sometimes are prepared by *in situ* sulfidation of supported Ni species. Under these conditions the sulfidation can be incomplete and along with Ni sulfides other Ni-containing species may be present in the sorbent. To compare their reactivity with that of NiS, we performed additional experiments with alumina-supported Ni^0 and NiO under the same conditions as for NiS (Fig.8). It follows that the chemical nature of Ni phase has a strong impact on the reactivity towards $AsPh_3$. Metallic Ni is the most reactive phase, while NiO shows only a very weak activity in $AsPh_3$ trapping. This difference can be attributed to a well-known strong hydorgenolysis activity of

metallic Ni [17]. Addition of non-metallic elements (S or P) on the Ni surface results in attenuation of this activity due to lowering of the electronic density on Ni atom and therefore weaker interaction with adsorbed species [18]. The trend observed in Fig.8 can be explained by the same phenomenon. Appearance of sulfur in Ni environment (in NiS) results in a slight lowering of reactivity in comparison with metallic Ni. Further decrease of electronic density on Ni atoms in NiO reduces dramatically its hydrogenolysis activity and therefore its reactivity in $AsPh_3$ decomposition.

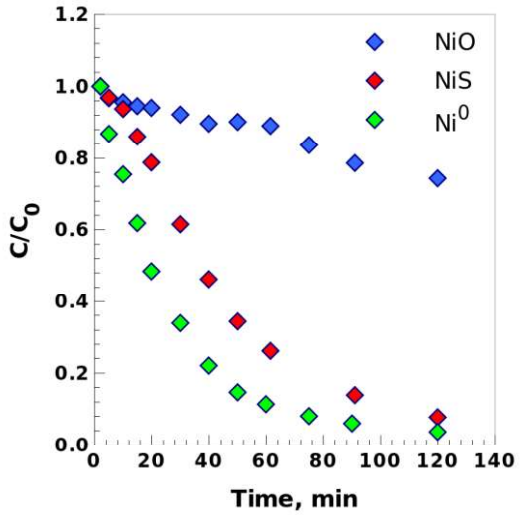

Figure 8 $AsPh_3$ conversion as a function of time for different Ni phases supported on γ-Al_2O_3 ($AsPh_3$ initial concentration – 28.6 mmol.L^{-1}, As/Ni = 1, 230°C, 23 bar H_2).

The dramatic drop of reactivity when going from NiS to NiO has an important practical implication. It suggests that for obtaining an active trapping mass the high sulfidation degree must be achieved in order to avoid the presence of residual NiO. This could be done, for example, using preferentially *ex situ* sulfidation under high H_2S concentration instead of *in situ* sulfidation procedure.

The second parameter, composition of As-containing species, is important since in the treated feedstocks various As-containing molecules were detected which contain different aliphatic and aromatic ligands [19]. It would be useful therefore to evaluate the impact of composition of As species on their decomposition rate. To do so we studied under similar conditions the trapping of triethyarsine ($AsEt_3$). The obtained conversion curves (Fig.9) show that at 230°C $AsEt_3$ is very difficult to decompose and only increase of temperature to 260°C allows to obtain a measurable

conversion. This dramatic difference of reactivity between $AsEt_3$ and $AsPh_3$ can be explained in terms of relative stability of -Et and -Ph ligands. The higher stability of - Ph intermediates in comparison with -Et ones (due to resonance effect) should facilitate As-C bond rupture in the case of $AsPh_3$ and make more rapid the overall reaction.

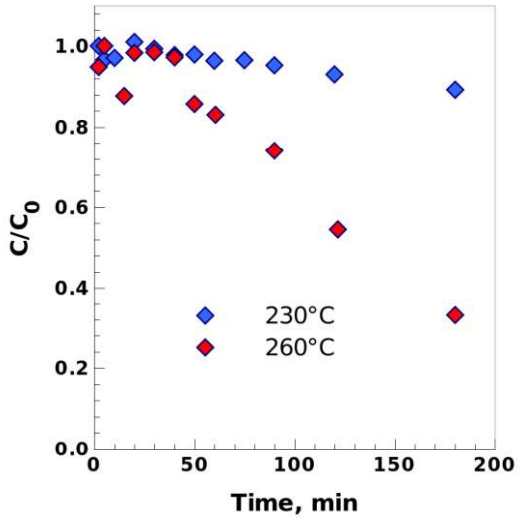

Figure 9 $AsEt_3$ conversion as a function of time in the reaction with NiS/γ-Al_2O_3 at 230 and 260°C ($AsEt_3$ initial concentration – 28.6 mmol.L^{-1}, As/Ni = 1, 23 bar H_2).

3.4 Role of the solid phase diffusion in $AsPh_3$ trapping

The analysis of the conversion curves of $AsPh_3$ for different As/Ni ratios shows that the decrease of concentration is linear at the beginning of the reaction, but becomes slower at the end (Fig.S3). This change means that at the beginning of the reaction the rate of reaction is constant but it declines when reaction proceeds. Such a decrease of the decomposition rate in a batch reactor can have one of two following reasons or their combination. First, it can be provoked by the decrease of the concentration of reacting species with time. Second, in our case it can be related to the formation of NiAs product layer creating a diffusion barrier for the reaction. Since these two effects occur simultaneously, the analysis of the standard conversion curves does not allow to distinguish which one is responsible for the decrease of the reaction rate.

To clarify this important point we performed additional experiments in which As/Ni ratio was equal

to 1, but $AsPh_3$ was added to the reactor in four successive doses. After injection of each dose we waited until a complete transformation of added $AsPh_3$ (~ 2 h) and then the next dose was injected (Fig.S4). The comparison of the obtained conversion curves shows that for three doses of $AsPh_3$ they are very close and only for the fourth dose the reaction rate declines (Fig.10). This finding shows that the presence of NiAs layer slows down the reaction only after the transformation of three injected doses which corresponds to conversion of ~ 50 % of Ni into NiAs. Below this value $AsPh_3$ transformation rate is not limited by diffusion through NiAs layer.

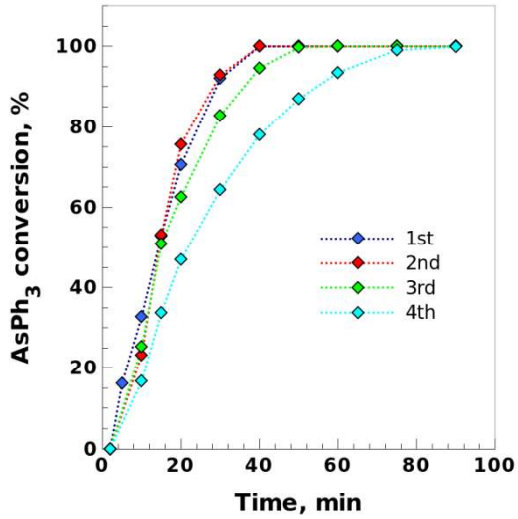

Figure 10 Conversion of $AsPh_3$ in the reaction with NiS/γ-Al_2O_3 as a function of time for successive injected doses (total As/Ni = 1, 230°C, 23 bar H_2). The lines are guides for the eyes.

The absence of diffusion limitations in solid transformation up to 50 % of conversion is a rather unexpected result. Its origin in our system can be understood using the shrinking core model of solid phase transformation [20]. For a spherical particle of initial radius R this model gives the following relationship between the product layer thickness (Δr) and the transformation degree:

$$\Delta r = R\left(1 - (1 - X)^{1/3}\right)$$

Using the values R = 4.5 nm (NiS average crystallite size is 9 nm, section 3.1) and X = 0.5 one can obtain that the thickness of the formed NiAs layer is about 0.9 nm. The obtained value is an estimation since some factors were not taken into account such as the size dispersion of NiS

crystallites or the presence of NiO phase. Nevertheless the obtained value suggests that even after conversion of 50 % of the active phase the product layer consists of very small crystallites. Due to this fact the formed NiAs layer should contain a large number of grain boundaries providing pathways for fast diffusion similarly to other solid state transformations [21].

If the diffusion through NiAs layer is not a rate determining step for conversion degree below ~ 50 %, the question arises about the nature of this step. Unfortunately, the batch reactor used in the present study does not allow a detailed kinetic analysis which can be applied for the measurements realized at the constant concentration [20]. However our data allow to formulate some hypotheses. Thus, the replacement of S by As on the surface (first step of NiS transformation), cannot represent the rate determining step since its rate should depend on the S/As ratio at the surface and therefore on the conversion degree. More generally, the fact the rate of $AsPh_3$ decomposition is independent of the sorbent conversion allows to suggest that the rate determining step does not involve solid modification. It should therefore be related to the transformation of the organic substrate - $AsPh_3$. Possibly it consists in As-C hydrogenolysis allowing to release As atoms which replace S atoms in NiS structure. We do not have direct evidence proving this hypothesis, but it is in line with the much lower reactivity of $AsEt_3$ (see section 3.3).

For conversion degrees higher than 50 % diffusion through NiAs layer starts to contribute to the slowdown of the reaction. In addition, NiO particles present in our sorbent react at high conversion, but at much lower rate than NiS (see section 3.3). The change of the reaction mechanism at ~ 50 % of conversion for the experiment with initial As/Ni=1 corroborates with a sharp decrease of the transformation rate observed after this value (see Fig. 4).

3.5 Mechanism of $AsPh_3$ decomposition on NiS

As we mentioned in section 3.2 the concentrations of the reaction products in the liquid phase vary with time in a complex manner (see Fig.4). While the concentration of benzene increases, those of thiophenol and diphenylsulfide pass through the maximum but not at the same time. In this section

we will sketch a possible mechanism of $AsPh_3$ decomposition allowing to explain these trends.

The first question concerns the possible relationship between the observed variation of the concentrations and the appearance of the diffusion limitations after 50 % of Ni conversion. For the experiment with the initial As/Ni = 1 such correlation seems to exist since the maximum of thiophenol concentration is indeed observed at ~ 50 % of $AsPh_3$ (and Ni) conversion (see Fig.4). However, during the test with the initial ratio As/Ni = 0.4 the trend for thiophenol is the same (Fig.11), but the maximum concentration is reached at ~ 40 min after decomposition of 73% of $AsPh_3$ which corresponds to conversion of 29 % of Ni. For the tests with As/Ni = 0.2 this value is even lower: the maximum in thiophenol concentration is observed after only ~ 15 % of Ni being transformed (Fig.S5). We conclude thus that the observed variation of the products concentration is not correlated with the changes in the sorbent composition. These trends should therefore be explained by interconversion of different species in H_2 atmosphere in the presence of $NiS/\gamma\text{-}Al_2O_3$.

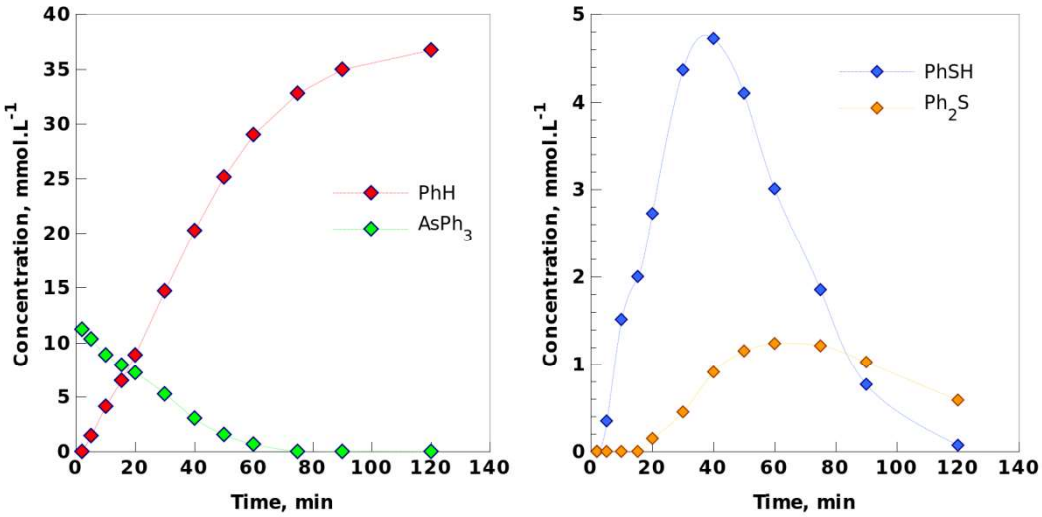

Figure 11 Time evolution of the concentrations of $AsPh_3$ and of the reaction products in the liquid phase during reaction of $AsPh_3$ with $NiS/\gamma\text{-}Al_2O_3$ (initial As/Ni ratio – 0.4, 230°C, 23 bar H_2). The lines are guides for the eyes.

In the following we will describe the possible processes taking place at different stages of the reaction between $AsPh_3$ and NiS. Our analysis is based on the data obtained for As/Ni=0.4 for two reasons. First, the concentrations of all products are sufficiently high to be measured accurately.

Second, in this case the amount of NiS in the sorbent is sufficient to capture all As and therefore the interaction with much less reactive NiO can be neglected.

The reaction can be divided in three distinct ranges (Fig.11). The first one extends from the beginning up to 40 min when the maximum of thiophenol concentration is achieved. Simultaneous formation of PhH and PhSH shows that the main reaction in this range is:

$NiS + AsPh_3 + 3/2H_2 \rightarrow NiAs + 2PhH + PhSH$ (1)

However, the ratio PhH/PhSH observed in this range (~ 3.3) is higher than that predicted by reaction (1). It means that another reaction producing only PhH occurs at the same time:

$NiS + AsPh_3 + 5/2H_2 \rightarrow NiAs + 3PhH + H_2S$ (2)

The absence of Ph_2S at the beginning of the reaction shows that it is a secondary reaction product forming possibly from PhSH when its concentration is sufficiently high:

$2PhSH \rightarrow Ph_2S + H_2S$ (3)

The second range is observed from 40 min to 75 min, the high limit corresponding to the disappearance of $AsPh_3$. The fact that the decrease of thiophenol concentration is accompanied by the increase of that of Ph_2S signifies that reaction (3) proceeds at this stage. In the same time benzene concentration continues to increase due to reaction (2) and also possibly via desulfurisation of PhSH and Ph_2S:

$PhSH + H_2 \rightarrow PhH + H_2S$ (4)

$Ph_2S + 2H_2 \rightarrow 2PhH + H_2S$ (5)

The occurrence of these reactions in our case is confirmed by the fact that after the complete transformation of $AsPh_3$ (75 – 120 min) the sulfur-containing species disappear and benzene concentration continues to rise (Fig.11). It is worth noting that reactions (4), (5) and possibly (3) need a catalyst to proceed under the used conditions. They occur therefore on the surface of the trapping mass and may thus compete with the reactions involved in $AsPh_3$ decomposition. Given the high concentration of formed PhSH (e.g. at 40 min it is higher than that of $AsPh_3$, Fig.11), these reactions can contribute to the slowing down of $AsPh_3$ decomposition at the high conversion

degrees.

3.6 Kinetic model of $AsPh_3$ decomposition

As detailed previously, the $AsPh_3$ conversion pattern follow the same trend for all As/Ni ratio, with a constant rate at the beginning of the experiment, and a decreasing rate at the end (Fig.S3). Thus, a simple kinetic model, using zero or first order with respect to $AsPh_3$, is not able to describe properly these conversion profiles. A partial order with respect to $AsPh_3$ should yield a better fit, however, it will not be able to describe correctly this peculiar pattern, corresponding to the change of the reaction order from zero to one.

Before discussing the kinetic model, the role of H_2 should be evaluated since it is involved in almost all mentioned reactions. To do so, we performed an additional test at 10 bar of H_2 instead of 23 bar used in all described experiments and we found that the conversion profiles are very similar (Fig.S6). This result shows that under high H_2 pressure, used in our study, the amount of active hydrogen species participating in the reaction is not a limiting factor whatever their exact nature. Therefore our model does not include H_2 pressure explicitly.

Taking into account the complex network of reactions involved in $AsPh_3$ decomposition, we can hardly apply the detailed classical kinetic models. We propose therefore a simplified kinetic model based on the reversible adsorption of $AsPh_3$ followed by its decomposition considered as a one-step reaction of the first order:

$$AsPh_3(liq) \overset{\frac{k_1}{k_{-1}}}{\leftrightarrow} AsPh_3(ads) \overset{k}{\rightarrow} Products$$

We assume that the rate determining step of reaction is the decomposition of adsorbed $AsPh_3$. In this case the surface reaction rate can be written in the following way:

$$r_S = -\frac{1}{S_{act}}\frac{dN(AsPh_3)}{dt} = -\frac{d[AsPh_3(ads)]}{dt} = k[AsPh_3(ads)] = k\theta N_M \quad \{1\}$$

Where r_S (mol·m^{-2}·s^{-1}) is the surface reaction rate, S_{act} (m^2) is the active surface area of the trapping mass, N($AsPh_3$) (mol) is the amount of transformed $AsPh_3$, k (s^{-1}) is the decomposition rate constant, [$AsPh_3$(ads)] (mol·m^{-2}) is the surface concentration of $AsPh_3$, θ is the surface fraction occupied by $AsPh_3$, N_m (mol·m^{-2}) is the $AsPh_3$ monolayer adsorption capacity.

Application of the steady state approximation to [$AsPh_3$(ads)] gives:

$$\frac{d[AsPh_3(ads)]}{dt} = 0 = k_1[AsPh_3](1-\theta)N_M - k_{-1}[AsPh_3(ads)] - k[AsPh_3(ads)] =$$

$$k_1[AsPh_3](1-\theta)N_M - k_{-1}\theta N_M - k\theta N_M \qquad \{2\}$$

Where [$AsPh_3$] (mol·m^{-3}) is the liquid phase concentration of $AsPh_3$, k_{-1} (s^{-1}) is the desorption rate constant and k_1 (m^3·mol^{-1}·s^{-1}) is the adsorption rate constant.

Using this equation the surface coverage θ can be determined:

$$\theta = \frac{k_1[AsPh_3]}{k_{-1} + k + k_1[AsPh_3]} \qquad \{3\}$$

The surface reaction rate can thus be expressed as:

$$r_S = k\theta N_M = \frac{K_1[AsPh_3]}{1 + K_2[AsPh_3]} \qquad \{4\}$$

with :

$$K_1 = kN_M\frac{k_1}{k_{-1}+k} \qquad K_2 = \frac{k_1}{k_{-1}+k}$$

To obtain the values of K_1 and K_2, the rate of the surface reaction must be related to the measured rate of $AsPh_3$ disappearance in the liquid phase (volume reaction rate). This relationship can be obtained using the fact that both the surface and the volume reaction rates correspond to the transformation of the same amount of $AsPh_3$:

$$r_V = -\frac{d[AsPh_3]}{dt} = -\frac{1}{V_{sol}}\frac{dN(AsPh_3)}{dt} = \frac{S_{act}}{V_{sol}}\ r_S = Ar_S \qquad \{5\}$$

Where r_V (mol·m^{-3}·s^{-1}) is the volume reaction rate, V_{sol} (m^3) is the volume of solution. It follows from equation {5} that the rate of reaction measured in solution is proportional to the rate of the surface reaction. Unfortunately the value of the proportionality coefficient cannot be calculated since the active surface area (S_{act}) is not known. Combination of equations {4} and {5} results in the following expression for disappearance rate of $AsPh_3$ in solution:

$$r_V = -\frac{d[AsPh_3]}{dt} = \frac{AK_1[AsPh_3]}{1 + K_2[AsPh_3]} = \frac{K_1'[AsPh_3]}{1 + K_2[AsPh_3]} \qquad \{6\}$$

Where K_1' (s^{-1}) is the new constant which includes the proportionality coefficient A.

With such equation, the reaction order depends on the concentration of $AsPh_3$ in the liquid phase: at high concentration (at the beginning of the reaction) the reaction order is zero ($r \sim K_1'/K_2$), whereas at the end of the reaction, the order is one ($r \sim K_1'\ [AsPh_3]$). Table 2 gives the optimized values of K_1' and K_2 which allow the best fit of the data for the different experiments and Fig.12 compares the experimental data with the optimized model fits. It can be concluded that similar values of K_1' and K_2 are obtained for the experiments where As/Ni ratio is smaller than one. In contrast for the experiment where As/Ni = 1, the constants are one order of magnitude lower, which may be due to appearance of other phenomena which slow down the reaction. As detailed previously, for As/Ni ratio higher than 0.5 diffusion through formed NiAs layer becomes slower and might decrease the overall reaction rate. Also, the presence of less reactive NiO can play the same role.

Table 2 Constants of equation {6} obtained from the fit of the experimental conversion profiles for different As/Ni initial ratios

As/Ni initial molar ratio	$K_1' \cdot 10^3$ **(s^{-1})**	K_2 **(L.mmol^{-1})**
1	0.43	0.012
0.4	3.0	0.75
0.2	2.3	0.75
0.1	2.4	0.85
0.05	3.2	0.80

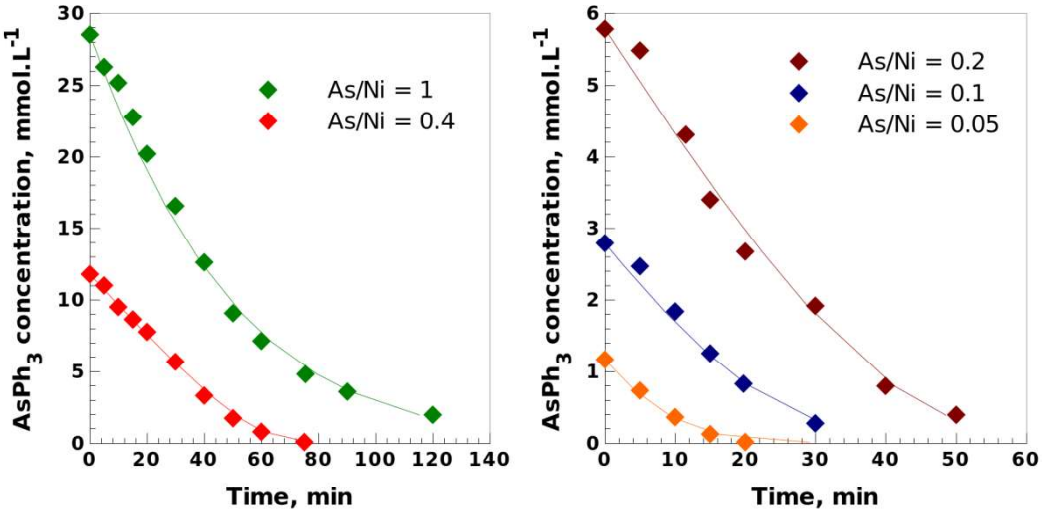

Figure 12 $AsPh_3$ conversion profiles for different initial As/Ni ratio (230°C, 23 bar H_2). Points are the experimental data, lines are the fits with equation {6} using the parameters given in Table 2.

4. Conclusions

In the context of trapping of As-containing species in petroleum feedstocks we studied reaction between $AsPh_3$ and NiS/Al_2O_3. The rate of disappearance of $AsPh_3$ was measured in a batch reactor in toluene solution at 230°C under 23 bar of H_2. The experiments were performed for different $AsPh_3$ concentrations (1.1 – 28.6 $mmol.L^{-1}$) and constant $NiS/\gamma\text{-}Al_2O_3$ amount corresponding to variation of As/Ni ratio in the range 0.05 - 1. These kinetic measurements and additional experiments allowed to determine the following main features of the reaction mechanism:

- The end reaction products are: NiAs, benzene and H_2S. The intermediate products, thiophenol and diphenylsulfide, were also observed in the liquid phase during reaction.
- For Ni conversion below ~ 50 % the diffusion through formed NiAs layer is not the rate determining step. Under these conditions the hydrogenolysis of C-As bonds appears to be the rate determining step.
- The decomposition of $AsPh_3$ follows the conversion profile with the rate order changing from zero at the beginning of reaction to one at the end. This trend is successfully described by a proposed kinetic model based on the decomposition of adsorbed $AsPh_3$.

- The reactivity of NiO towards $AsPh_3$ is much lower than that of NiS. This fact highlights the importance of a complete sulfidation of As trapping masses.

An important general point revealed by our study concerns the fact that a stoichiometric NiS – NiAs transformation involves a key catalytic step. The decomposition of As molecular species (producing As atoms) occurs through their heterogeneous catalytic reaction with H_2. Moreover, at low conversion this catalytic reaction becomes a rate determining step which results in a strong difference in reactivities of NiS towards $AsPh_3$ and $AsEt_3$. The presence of this catalytic step explains also a much lower reactivity of NiO in comparison with NiS.

Acknowledgments

We thank Remi Chassagnon and Olivier Heintz (Laboratoire Interdisciplinaire Carnot de Bourgogne) for performing HRTEM and XPS measurements.

References

1. J.B. Stigter, H.P.M. de Haan, R. Guicherit, C.P.A. Dekkers, M.L. Daane, Environ. Pollut. 107 (2000) 451.

2. A. de Jesus, A.V. Zmozinski, I.C.F. Damin, M.M. Silva, M.G.R. Vale, Spectrochim. Acta B 66 (2012) 86.

3. B. Bouyssiere, F. Baco, L. Savary, H. Garraud, D. L. Gallupe, R. Lobinski, J. Anal. At. Spectrom. 16 (2001) 1329.

4. M. D. Argyle, C. H. Bartholomew, Catalysts 5 (2015) 145.

5. B. Nielsen, J. Villadsen, Appl. Catal. 11 (1984) 123.

6. R. N. Merryfield, L. E. Gardner, G. D. Parks, in: M. L. Deviney, J. L. Gland (Eds.), Catalyst Characterization Science, ACS Symposium Series, 1985, p.2-14.

7. A. Puig-Molina, L. P. Nielsen, A. M. Molenbroek, K. Herbst, Catal. Lett. 92 (2004) 29.

8. S. Yang, J. Adjaye, W. C. McCaffrey, A. E. Nelson, J. Mol. Catal. A: Chem. 321 (2010) 83.

9. Picard, F; Coupard, V.; Bouchy, C. French Patent FR2876113 B1 (2008).

10. B. Didillon, L. Savary, Y. A. Ryndin, J.-P. Candy, J.-M. Basset, C. R. Acad. Sci. Paris, Serie IIc, Chimie: Chemistry 3 (2000) 413.

11. Y. A. Ryndin, J.-P. Candy, B. Didillon, L. Savary, J.-M. Basset, C. R. Acad. Sci. Paris, Serie IIc, Chimie : Chemistry 3 (2000) 423.

12. Y. A. Ryndin, J.-P. Candy, B. Didillon, L. Savary, J.-M. Basset, J. Catal. 198 (2001) 103.

13. V. Maurice, Y. A. Ryndin, G. Bergeret, L. Savary, J.-P. Candy, J.-M. Basset, J. Catal. 204 (2001) 192.

14. Y. A. Ryndin, J.-P. Candy, G. Bergeret, L. Savary, D. Uzio, J.-M. Basset, Stud. Surf. Sci. Catal. 139 (2001) 479.

15. D.L. Legrand, H.W. Nesbitt, G.M. Bancroft, American Mineralogist 83 (1998) 1256.

16. H. W. Nesbitt, M. Reinke, American Mineralogist 84 (1999) 639.

17. G. Leclercq, L. Leclercq, L. Bouleau, S. Pietrzyk, R. Maurel, J. Catal. 88 (1984) 8.

18. G. Wang, S. Zhang, X. Zhu, C. Li, H. Shan J. Ind. Eng. Chem. 86 (2020) 1.

19. P. Sarrazin, C. J. Cameron, Y. Barthel, M. E. Morrison, Oil and Gas Journal 91 (1993) 86.

20. J. Szekely, J.W. Evans, H.Y. Sohn, Gas-Solid Reactions, Academic Press, New York,1976.

21. J. Skrzypski, I. Bezverkhyy, O. Heintz, J.-P. Bellat, Ind. Eng. Chem. Res. 50 (2011) 5714.

Supplementary Material

Click here to access/download

Supplementary Material

SI_revised.pdf

*Credit Author Statement

Credit author statement

Angélique Jallais: Investigation ; Visualisation ; Formal analysis ; Writing - review & editing

Michel Thomas: Supervision; Conceptualization; Methodology; Funding acquisition; Writing - review & editing

Antoine Hugon: Supervision; Conceptualization; Methodology; Funding acquisition; Writing - review & editing

Igor Bezverkhyy : Methodology; Supervision; Writing - original draft; Writing - review & editing

*Declaration of Interest Statement

Declaration of interests

☒ The authors declare that they have no known competing financial interests or personal relationships that could have appeared to influence the work reported in this paper.

☐The authors declare the following financial interests/personal relationships which may be considered as potential competing interests:
